ELECTRICAL IMPEDANCE SPECTROSCOPY AS A NON-INVASIVE METHOD FOR EVALUATING PERFUSED EX-VIVO PORCINE KIDNEYS

Michiel van Hoeven

Machanical, Maritime and Materials Engineering, Delft University of Technology

BME51035: BME MSc Thesis

dr.ir. R.F. Remis, dr. M.A. Engelse, dr. ir. T.J.C. Oude Vrielink, M.J.A. de Haan

23 januari 2022

ELECTRICAL IMPEDANCE SPECTROSCOPY AS A NON-INVASIVE METHOD FOR EVALUATING PERFUSED EX-VIVO PORCINE KIDNEYS

Michiel van Hoeven 4291360

Abstract — **This research addresses the following question: *Is it possible to detect vascular obstructions and oedemas or monitor the decellularization process in perfused ex-vivo porcine kidneys using electrical impedance spectroscopy?* Patients on the waiting list for kidney transplantation die because of a kidney shortage. A part of this problem can be solved by prolonging the period of preservation between the removal of the kidney from the body and the transplantation. However, oedemas and vascular obstructions are more likely to occur with longer perfusions. The kidney donor risk index doesn't take this into account so a new technique needs to be established to assess the development of oedema and vascular obstruction. Another approach for increasing the supply of donor kidneys is de- and recellularization of the kidney. Electrical impedance spectroscopy shows promising results in the pancreas and this technique can probably be transferred to the kidney. EIS is a non-invasive, low cost, portable measuring technique that shows the results in real-time. A Spectra Bioimpedance and EIT Complete Kit with the 4-electrode attachment have been used at low frequencies (500 Hz) and high frequencies (70.000 Hz) for the evaluation of the porcine kidneys. Two different measurement techniques will be used, measurements through the renal artery and measurements on the kidney. These techniques are tested during the decellularization process, oedema formation, and vascular obstruction simulation to determine if impedance changes can signal these defects in the kidney. Robust changes have been made to the porcine kidneys in this regard. The sensitivity of the methods is less than expected. Only the decellularization results showed a notable change over time. The conclusion of this research is therefore: The results cannot prove a clear connection between vascular obstruction and oedema detection and electrical impedance changes. There is a probable correlation between electrical impedance and the phase of decellularization in which the kidney is in. Follow-up research is needed to substantiate this further.**

Keywords: *electrical impedance spectroscopy – kidney perfusion – vascular obstruction – oedema formation - decellularization.*

I. INTRODUCTION

Kidney transplantation is at present the best therapy for patients with end-stage kidney failure [1]. Patients with a kidney transplant have a longer life expectancy than patients on dialysis. People with a donor kidney from a deceased donor live an average of 10 years without needing dialysis or another transplant and patients with a kidney from a living donor live an average of 20 without needing dialysis or another transplant [2]. However, 67 patients of the 831 patients on the waiting list died before they could receive a donor kidney in 2018 [2]. There is a shortage of donor kidneys, even with transplanting kidneys from deceased donors as well as living donors.

It has been hypothesized that the availability of donor kidneys can be increased by prolonging the period of preservation between the removal of the kidney from the body and the transplantation. Machine perfusion can be used to keep kidneys alive outside of the body for extended periods [3]. The key attributes of machine perfusion are to provide an environment that is protective to the organ, ensures optimal oxygen delivery, and supports metabolic function [4].

The current way to assess kidneys is the Kidney Donor Risk Index (KDRI). This index combines a variety of donor factors to encapsulate the risk of graft failure after kidney transplantation into a single number [5]. Graft failure can be defined as the failure of the organ to operate in the receiving patient. The value for the KDRI is calculated using the characteristics of the donor's age, height, weight, ethnicity, history of hypertension, history of diabetes, cause of death, serum creatinine, Hepatitis C Virus (HCV) Status, from serological or NAT testing, and Donation after Circulatory Death (DCD) Status. These characteristics are multiplied with a coefficient and added together to form the definitive KDRI value [6].

However, the KDRI focuses on the success of the transplantation and not the state of the kidney beforehand, during perfusion. A novel method has been proposed by Hosgood et al. [7]. This method grades kidneys using a quality assessment score (QAS). The QAS relies on macroscopic appearance in other words the surgeon's eye. This is a subjective assessment. It doesn't take into account the forming of oedemas or vascular obstructions in the kidney in an objective manner. These characteristics are hard to assess but

2

can have serious consequences. Both of these characteristics precede necrosis [8]. The study of Pool et al. measures an increase in weight of all kidneys after 7-hour normothermic machine perfusion [3]. This rapid increase in weight is likely due to an accumulation of extracellular fluid in tissue and thus the formation of oedema. Longer perfusions will probably result in even higher chances of oedema formation. This could cause oedema formation to be a serious problem for transplanting kidneys that have had prolonged perfusions before transplantation.

Another process that can help the kidney shortage is the decellularization and recellularization of kidneys. The cells of a kidney are first rinsed out of the kidney and replaced by stem cells to generate personalized grafts [9]. The primary way to assess if decellularization was successful at the moment is to cut open the kidneys and take samples [10]. This defeats the purpose of keeping the extracellular matrix intact for recellularization. A better way to assess the decellularization process would be by using an ex-vivo non-invasive technique, a technique that operates from outside of the kidney without harming it.

A possible solution for assessing the presence of oedemas or vascular obstructions in the kidneys and the efficiency of the decellularization process is the use of electrical impedance spectroscopy. Electrical impedance spectroscopy (EIS) shows changes in impedance in the interior of a medium by measuring the voltage between electrodes positioned on the body surface, as a set current runs through the medium at a specified frequency band [11]. EIS is currently used in finding malignant tumours in the breast area, determining the length of the root canal in dental health, the drug efficacy for ALS patients, and the study of damage to the stomach and small intestines [9], [12]. EIS is non-invasive, is low cost, is non-ionizing, is radiation-free, shows the results in real-time and is portable [13], [14]. This causes EIS to be a superior technique for kidney transplantation (a field that needs quick and portable techniques) compared to other measurement techniques that produce a higher resolution measurement but take more time [13]. EIS can detect the impedance of the extracellular fluid, the intracellular fluid and the cell membrane [13]. Changes in the ratio between intra- and extracellular fluid can be indicators of vascular obstruction and oedema formation while a decrease in cell membranes can show a successful decellularization process. The study of [8] concludes that electrical impedance tomography, a technique that uses multiple EIS signals, is the best tool to non-invasively assess oedemas in an ex-vivo pancreas. This is a promising result and suggests that this can also be used to assess oedemas in kidneys. The overall research will therefore focus on the following question: *Is it possible to detect vascular obstructions and oedemas or monitor the decellularization process in perfused ex-vivo porcine kidneys using electrical impedance spectroscopy*?

II. METHOD

A. How does Electrical Impedance Spectroscopy work?

Electrical impedance spectroscopy (EIS) is a non-invasive, low-cost measuring technique that communicates the results in real-time and is portable [13], [14]. EIS calculates changes in impedance in the interior of a medium by measuring the voltage between electrodes positioned on the surface of the body, using a sinusoidal current that runs through the medium at a specified frequency band [11] as seen in **Figure 1**.
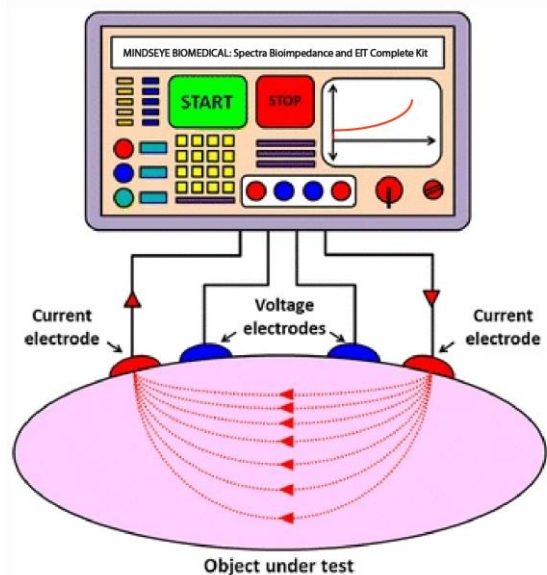

Figure 1. Electrical impedance schematic. The voltage is measured at a specified sinusoidal current that runs through the medium [11].

The analysis of these EIS signals is the first step to visualising the inside of the kidneys. Multiple EIS signals sent between a network of multiple electrodes can be combined using an algorithm to create an electrical impedance tomography (EIT). The best algorithm for this at the moment is the Graz Consensus. **Appendix 1** discusses this in more detail with the accompanying mathematics. This research focuses on the EIS method as it was not possible to reprogram the Spectra Bioimpedance and EIT Complete Kit (Mindseye Biomedical) to use the EIT method with measurements through the artery.

The components in the living tissue that influence the impedance of the tissue are the extracellular fluid, the intracellular fluid and the cell membrane. The impedance measured by the EIS signal is composed of two components, the resistance (R) which is caused by the extracellular fluid and the reactance (X_c) that is caused by the capacitance of the cell membrane and intracellular fluid [15]:

$$Z = R + jX_c$$

(eq. 1)

$$|Z| = \sqrt{R^2 + X_c^2}$$

(eq. 2)

Where the resistance is determined by the object's shape expressed in terms of length (L) and area surface (A), and

3

the material type, that is defined as resistivity (**ρ**), as demonstrated in **Equation 3**. The reactance of an object is described by resistance to voltage variation across the object and is inversely related with signal frequency (**f**) and capacitance (**C**), as shown in **Equation 4** [15]. The capacitance is defined as the ability of the non-conducting object to save electrical charges, that is equal to the ratio between differentiation in voltage across object ($\frac{dV}{dt}$) and current that is passed through the object ($I(t)$), as demonstrated in **Equation 5** [15]. This is why the impedance of tissue is voltage, current and frequency dependant.

$$R = \rho \frac{L}{A}$$

(eq. 3)

$$X_c = \frac{1}{2\pi f * C}$$

(eq. 4)

$$C = \frac{dV}{dt} / I(t)$$

(eq. 5)

On a physiological level, the low frequency waves can´t travel through the cell membrane and will therefore travel around the cells through the extracellular fluid around the living cell tissue [11]. The high frequency waves can travel through the cell membrane and will therefore take the shortest path through the extracellular fluid, the cell membrane and the intracellular fluid as shown in **Figure 2** [11], [16].
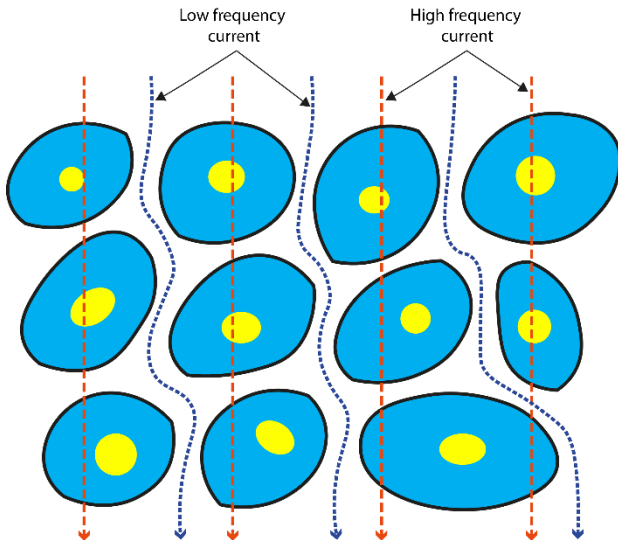

Figure 2. The frequency-dependent impedance properties of biological tissues. Low frequencies will travel solely through the extracellular fluid. High frequencies will travel through extracellular fluid as well as the cell membrane and intracellular fluid [11].

The equivalent circuit of tissue can be represented as an extracellular resistance that is in a parallel circuit with a cell membrane capacitor and an intracellular resistance as shown in **Figure 3** [17].
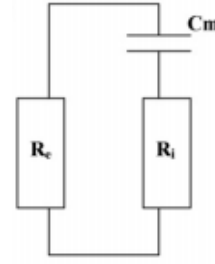

Figure 3. Equivalent circuit of living tissue with the extracellular resistance (Re), the cell membrane capacitance (Cm), and the intracellular resistance (Ri) [17].

The cell membranes act as capacitors at intermediate and low frequencies [17]. At low frequencies, the membrane capacitance produces very high capacitive reactance, which in turn develops a very high impedance across the cell and hence does not allow the electrical signal to pass through. On the contrary, at high frequencies, the capacitive reactance of the cell membrane becomes low which easily allows the current to pass through the cells by penetrating the cell membranes [13]. This is the reason that the extracellular fluid on its own must be measured at low frequencies (< 1kHz) and that the best representation of intra- and extracellular fluid combined is at very high frequencies (> 5 MHz) [17]. At intermediate frequencies, the capacitance of the cell membrane will interfere unpredictably. A formula can be derived from the equivalent circuit to confirm these statements. First, the equation of the impedance of a capacitor and resistor are needed [18]:

$$Z_R = R$$

(eq. 6)

$$Z_C = \frac{1}{j\omega C}$$

(eq. 7)

With **Z** the impedance, **R** the resistance, **j** the imaginary unit, **ω** the frequency, and **C** the capacitance. Calculating the equivalent impedance for the intracellular fluid and cell membrane capacitance together gives the equation [18]:

$$Z_{int} = Z_{Ri} + Z_{Cm} = R_i + \frac{1}{j\omega C_m} = \frac{R_i j\omega C_m + 1}{j\omega C_m}$$

(eq. 8)

Combining the intracellular and extracellular impedances delivers the following equation [18]:

$$\frac{1}{Z_{tissue}} = \frac{1}{Z_{int}} + \frac{1}{Z_{ext}} = \frac{1}{\frac{R_i j\omega C_m + 1}{j\omega C_m}} + \frac{1}{R_e}$$
$$= \frac{R_e j\omega C_m + R_i j\omega C_m + 1}{R_e(R_i j\omega C_m + 1)}$$

(eq. 9)

$$Z_{tissue} = \frac{R_e(R_i j\omega C_m + 1)}{R_e j\omega C_m + R_i j\omega C_m + 1}$$

(eq. 10)

Equation 10 demonstrates that at low frequencies (when $\omega \to 0$) the current essentially flows through the extracellular fluid (R_e). When the frequency increases extracellular fluid (R_e), the cell membrane (C_m), and intracellular fluid (R_i) all contribute to the impedance. Until the values of the frequency start to dwarf the other values and approach infinity, then the impedance will approach zero. This affirms what other studies found [11], [13], [17]–[20]. The values for the extracellular fluid, cell membrane capacitance and intracellular fluid for the same distance will change throughout the different experiments and influence the impedance. These changes should provide insight into the inner workings of the kidneys without the need to cut them open.

B. Experimental setup

The experiments to check for the presence of vascular obstructions and oedema´s in porcine kidneys and monitor the decellularization process will be done using the Spectra Bioimpedance and EIT Complete Kit (Mindseye Biomedical) with the 4 electrode attachment [21]. The settings of the device allow impedance measurements at frequencies of 200, 500, 800, 1.000, 2.000, 5.000, 8.000, 10.000, 15.000, 20.000, 30.000, 40.000, 50.000, and 70.000 Hertz. Especially the difference between the lowest and highest frequencies over time is of interest.

The porcine kidney used for the experiments will be procured from an abattoir, flushed with preservation solutions, and cooled and stored on ice for transport to the LUMC. At the LUMC, the kidneys will be prepared for their respective experiments.

1) Measurement on the kidney

The sending (current) electrodes and receiving (voltage) electrodes are placed on the surface of the porcine kidney and the signal is sent through the kidney tissue. This four-electrode technique has been used multiple times in electrical impedance spectroscopy studies [11], [13], [16], [16]–[20]. Three different paths are measured on the kidney as seen in **Figure 4**. The first path is through the whole kidney. The second path is through the part of the kidney that is the focus of the experiment. The third path is through the unchanged part of the kidneys and operates as a control measurement. Only path one was used for the decellularization process measurements because the whole kidney is the focus of those experiments.
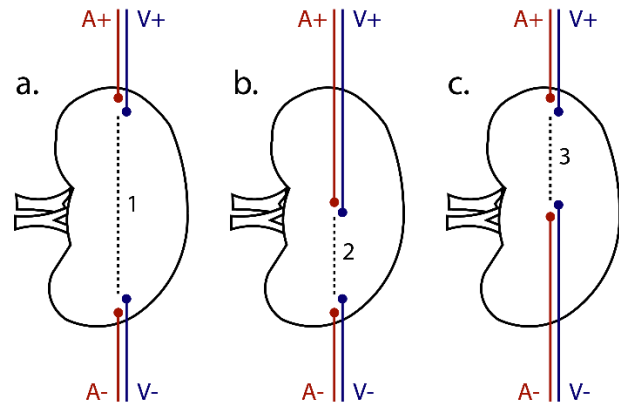

*Figure 4. Sending and receiving electrode placement on the porcine kidney. **a.** Path 1: Through the whole kidney. **b.** Path 2: Through the part experiencing changes. **c.** Path 3: Control*

2) Measurement through the renal artery

A novel method for measuring impedance through the kidney using spectroscopy was attempted during the experiments of this paper. Two electrodes, the V+ and A+ electrodes, are placed in the tubing connected to the renal artery. The two other electrodes, the V- and A- electrodes, are placed on the surface of the kidney as seen in **Figure 5**. The hypothesis behind this novel method is that the signal is allowed to travel through the perfusate in the arterial network and use it as a highway through the kidney tissue to reach the electrodes on the surface while traversing the least extracellular fluid, cell membranes, and intracellular fluid possible due to the lower impedance of the perfusate. This method could have a major impact in detecting the presence of vascular obstructions as the signal needs to leave the arterial network sooner than expected and traverse a greater distance through the tissue of the kidney thus increasing the impedance. Three different paths are measured through the renal artery as seen in **Figure 5**. The first path is through the middle of the kidney. The second path is through the part of the kidney that is the focus of the experiment. The third path is through the unchanged part of the kidneys and operates as a control measurement. Only path one was used for the decellularization process measurements.
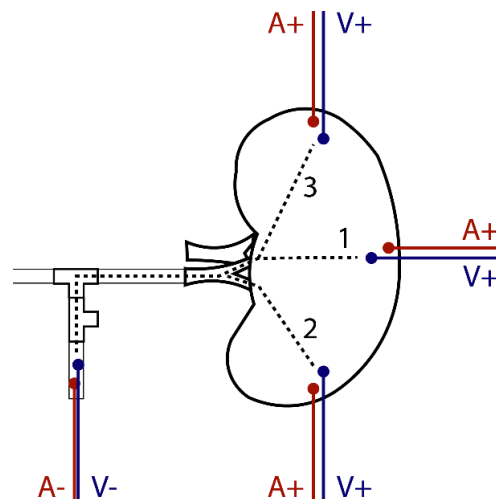

Figure 5. Sending and receiving electrode placement through the renal artery. Path 1: Through the middle of the kidney. Path 2: Through the part experiencing changes. Path 3: Control

C. The decellularization process

Acellular kidneys can be engineered by treating normal kidneys with detergents or enzymes, in a process that is called whole organ decellularization. These are robust changes to the structure of the kidney tissue. The resulting decellularized scaffold is composed of the extracellular matrix present within all organs and tissues [10], [22]. During the decellularization process, the detergents and enzymes demolish the cell membrane of the living cells and flush the dead cells out of the organ, leaving only the extracellular matrix of the kidney. The tissue will be composed of fewer and fewer living cells as the decellularization process continues as seen in **Figure 6**. **Figure 7** shows the predictive models for the decellularization process with measurements on the kidney and through the artery. The low high frequency impedances will drop a little due to a decrease in cells blocking its path. The high frequency impedances will drop significantly because of cell membrane capacitances and intracellular fluid resistances of the flushed cells that are replaced by the extracellular fluid resistance. The high frequency and low frequency impedance values will eventually be identical because only the extracellular fluid will remain in an ideal acellular kidney. This is supported by **Equation 10** (when $\mathbf{C_m} \to \mathbf{0}$ and $\mathbf{R_i} \to \mathbf{0}$ then $\mathbf{Z_{tissue}} = \frac{R_e}{1}$).
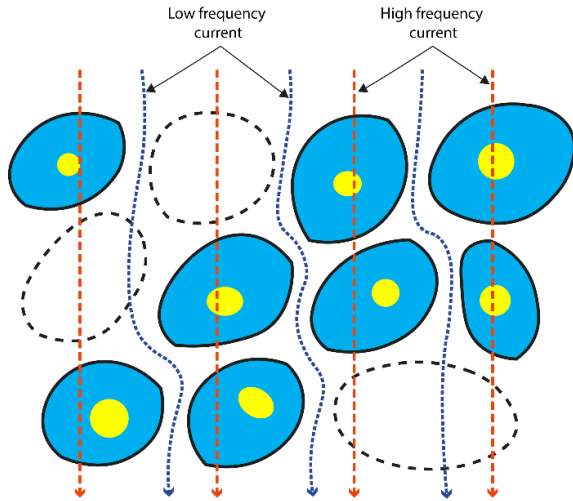

Figure 6. *The frequency-dependent impedance properties of biological tissues during the decellularization process. There is an increase of extracellular fluid due to the destruction of the living cells caused by detergents and enzymes.*
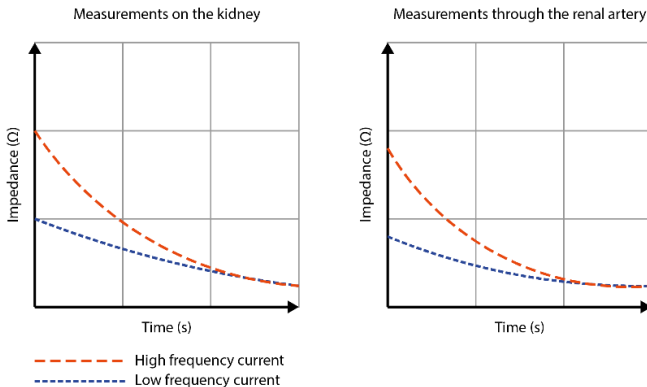

Figure 7. *Predictive models for the decellularization process. Left: The model on the kidney. Right: The model through the artery.*

The porcine kidney is placed in a custom made organ chamber as used in the study of Leuning et al. [10] and de Haan et al. [22]. This organ chamber protects the kidney against contamination. A pressure sensor-controlled centrifugal pump supplies the pressure to the system to control the flow through the tubing. The perfusate enters the renal artery and leaves the renal vein to be collected in the organs chamber. The perfusate is then pumped to an external basin and from there continues to be perfused through the kidney as seen in **Figure 8**. The fluid in the external basin is refreshed once a day to prevent saturation of the fluid and therefore diminish the efficiency of the decellularization process.
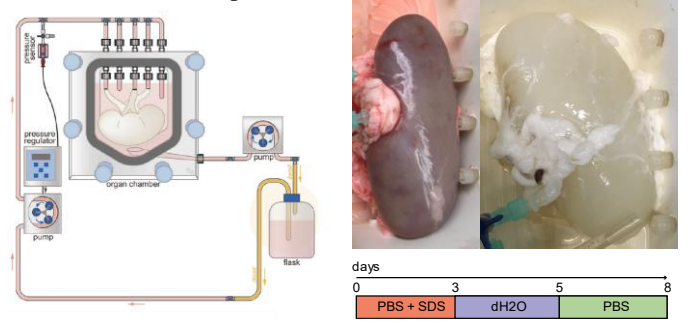

Figure 8. *Left: Setup of the decellularization process [22]. Upper right: Porcine kidney before and after decellularization. Lower right: The perfusate used during the decellularization process.*

The used method for organ decellularization has been reported previously by Song et al. and Leuning et al. [10], [23]. The porcine kidneys for the decellularization process experiments were flushed with PBS with heparin (500 IE/L) and the perirenal fat and kidney capsule were removed. The renal artery was cannulated with a Luer-lock connector (Cole-Parmer, Barendrecht, the Netherlands) and the kidney was perfused with 1% sodium dodecyl sulfate (SDS) (w/v) (Sigma Aldrich, Zwijndrecht, the Netherlands) in phosphate-buffered saline (PBS) containing 2% penicillin/streptomycin (Life Technologies, Europe Bleiswijk, the Netherlands), 6 µg/mL ciprofloxacin (Fresenius Kabi, Huis ter Heide, the Netherlands), 0.1% fungizone (w/v) (Bristol-Myers Squibb, Utrecht, the Netherlands), and 2500E DNAse (Pulmozyme, Roche, Woerden, the Netherlands) under a constant pressure of maximal 75 mm Hg for 3 days. Afterwards, the kidneys were perfused for 1 day with dH2O with antibiotics, antimycotics, and DNAse. Then the kidneys were flushed with 1% Triton-X 100 (v/v) (Sigma Aldrich) for 1 day afterwards flushed with PBS with antibiotics and antimycotics for at least 3 days, all under a constant pressure of max. 75 mm Hg. Kidneys were stored at 4°C in PBS until further use.

D. Oedema formation following overnight perfusion

The setup that is used for the oedema experiments to keep the ex-vivo porcine kidney alive after removal from the body is seen in **Figure 9**. It is a sub-normothermic machine perfusion circuit. Sub-normothermic machine perfusion continues the normal physiological processes and restoration of the ATP and tissue repair before transplantation [24]. Sub-normothermic perfusion is used instead of normothermic perfusion to decrease the oxygen demand and drop the need for oxygen carriers in the

perfusate. A pressure sensor-controlled centrifugal pump supplies the pressure to the system to control the flow through the tubing. Before entering the renal artery, perfusate passes through an oxygenator. A dialysis machine transfers the nutrition to the perfusate for the kidney. The kidney is placed in a custom made organ chamber as used in the study of Leuning et al. [10]. This circuit can keep the kidney alive for several days outside of the body and is closed off from the outside environment to prevent infections from occurring inside of the kidney. Gibco Dulbecco's Modified Eagle Medium: Nutrient Mixture F-12 (DMEM/F-12) (ThermoFisher, Waltham, USA) was used as a perfusate in combination with 40 g/l Alburex 20 (CSL Behring GmbH, Marburg, Germany) and the same antibiotics and antimycotics as were used in the decellularization process.
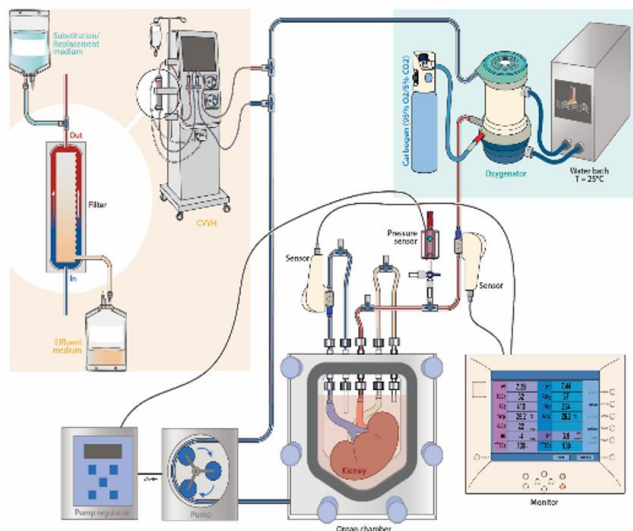

Figure 9. Setup of the sub-normothermic machine perfusion.

To induce the oedema formation after overnight perfusion, the renal capsule is cut open on one side of the porcine kidney. The renal capsule on the other side of the kidney is being kept intact for control readings during the experiment. The renal capsule is a tough fibrous layer that surrounds the kidney and helps support the kidney by applying a counterpressure [25]. By cutting the capsule and increasing the pressure through the system, the kidney on the cut side of the capsule will swell due to a lack of counter pressure. This swelling is caused by an accumulation of extracellular fluid, and thus an oedema formation. This is a robust modification to the kidney to achieve the maximum change in impedance for this phenomenon. Measurements are taken before oedema formation, directly after the renal capsule has been cut, and at the 1-hour, 2-hour, and 3-hour mark.

The prediction is that the oedema formation will cause an increase in extracellular fluid between the living cells. This will make it easier for the low frequency signals to travel in a straight line and thus travel a shorter distance through the extracellular fluid as shown in **Figure 10**. The high frequency signals will travel through more extracellular fluid and fewer cell membranes and intracellular fluid when moving the same distance through the tissue compared to a normal porcine kidney. The predictive model is therefore that the impedance of

both the low and high frequency signals will decrease when oedema is present as shown in **Figure 11**.
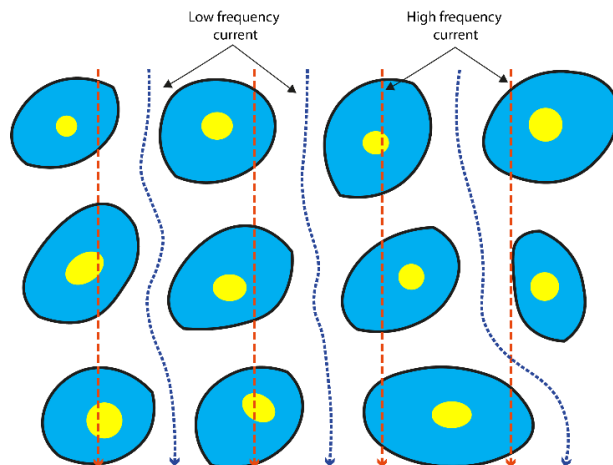

Figure 10. The frequency-dependent impedance properties of biological tissues during oedema formation. There is an increase in extracellular fluid due to the lack of counterpressure of the renal capsule.
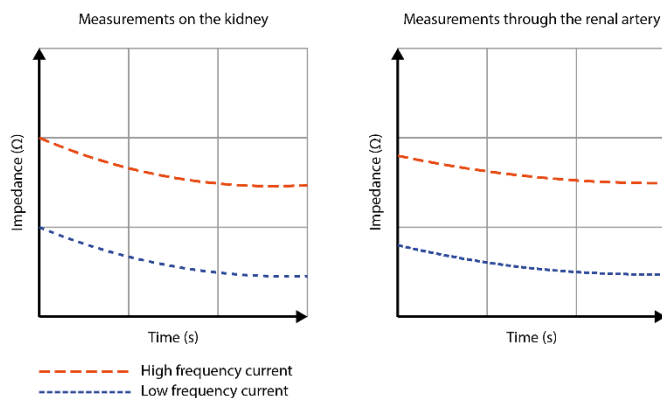

Figure 11. Predictive models during oedema formation. Left: The model on the kidney. Right: The model through the artery.

E. Vascular obstruction simulation following overnight perfusion

The vascular obstruction simulation experiments use the same setup for sub-normothermic machine perfusion as the oedema formation experiments. Given anatomical variation, the artery sometimes branches into two before entering the kidney. These kidneys are used for the vascular obstruction experiments. To simulate an excessive vascular obstruction of the artery, one of the two artery branches is closed by clamping a vascular clamp on that branch. The lack of patency through that branch and the corresponding half of the kidney is then confirmed by methylene blue perfusion. The part of the kidney that is supplied by the branch that is still open should show a blue discolouration. Measurements are taken before blocking the branch with the vascular clamp, directly after applying the blockade, and at the half-hour and hour mark. The vascular clamp is removed after an hour has passed. Measurements are then taken at the 10 minutes, hour, and 2-hour mark.

The prediction is that the blockade will cause a decrease in extracellular fluid between the living cells due to a lack of incoming perfusate. This will make it harder for the low

7

frequency signals to travel between the living cells as they are closer packet together. The high frequency signals will travel through less extracellular fluid and more cell membranes and intracellular fluid when moving the same distance through the tissue compared to a normal porcine kidney as seen in **Figure 12**. The predictive model is therefore that the impedance of both the low and high frequency signals will increase when a blockade is present. This increase in impedance will probably be much higher for the measurements through the artery because the signal can't use the arterial network as the shortest route through the kidney and has to travel through the open arterial branch followed by the intra- and extracellular fluid and the cell membranes of the kidney as shown in **Figure 13**.
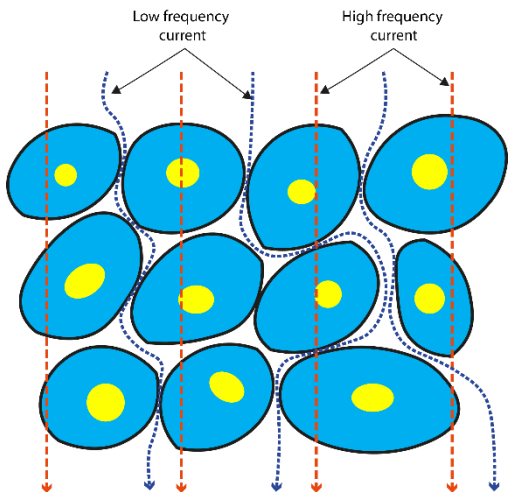

Figure 12. The frequency-dependent impedance properties of biological tissues during vascular obstruction simulation. There is a decrease in extracellular fluid due to an obstruction in the artery.
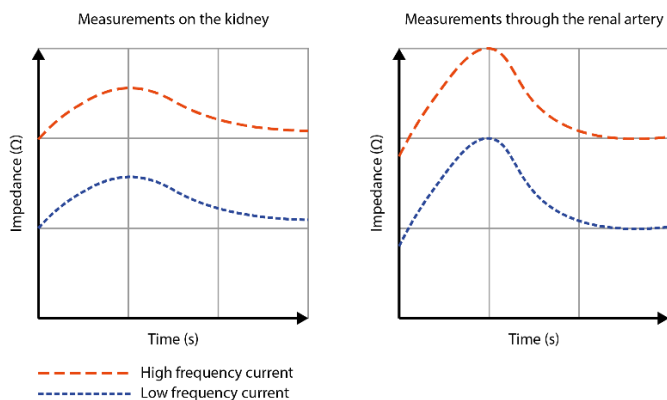

Figure 13. Predictive models during vascular obstruction simulation. The impedance increases while the vascular clamp is applied and decreases again after the clamp is removed. Left: The model on the kidney. Right: The model through the artery.

III. RESULTS

The Spectra Bioimpedance and EIT Complete Kit records the impedances over time at frequencies ranging from 200 to 70.000 Hertz and displays them in a graph as seen in **Figure 14**. The 200 Hertz measurements consistently show an increased impedance with a large standard deviation compared to the lower and stable measurements at 500, 800 and 1.000 Hertz. So, the 500 Hertz measurements were chosen to represent the low

frequencies over time in the analysis. The 70.000 Hertz measurements were chosen to represent the high frequencies over time given it being the upper constraint of the Spectra Bioimpedance and EIT Complete Kit. The penetration depth of a signal in a kidney at a frequency of 70.000 Hertz is 5.22 meters and should therefore not pose a problem [26].
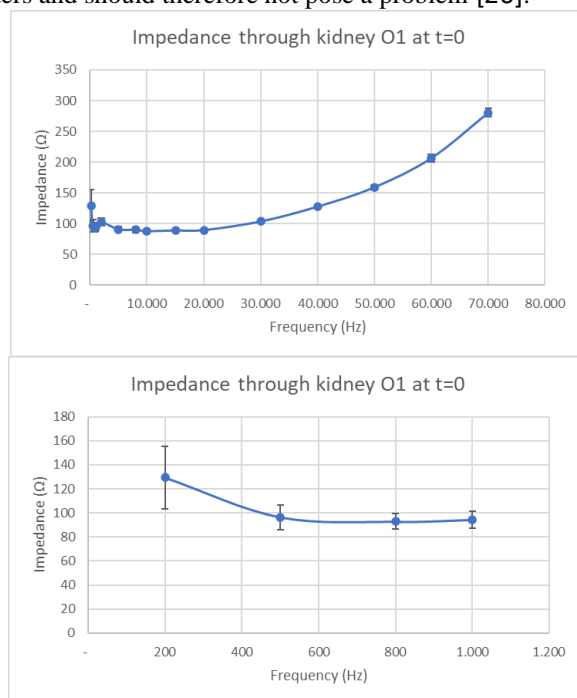

Figure 14. Upper: Output of the Spectra Bioimpedance and EIT Complete Kit at the start of the experiments on kidney O1, before cutting the renal capsule. Lower: Standard deviation of the low frequencies.

Blood has the same three-element equivalent circuit as the kidney tissue, where the red blood cells replace the cell membrane capacitance and intracellular fluid and the blood plasma replaces the extracellular fluid [27]. Tests have been performed to establish the impedance of combinations of blood and PBS at different frequencies as seen in **Figure 15**. A higher concentration of PBS can be interpreted as more extracellular fluid. The data from **Figure 15** can be found in **Appendix 10** and confirms that an increase in extracellular fluid will decrease the impedance of the tissue.
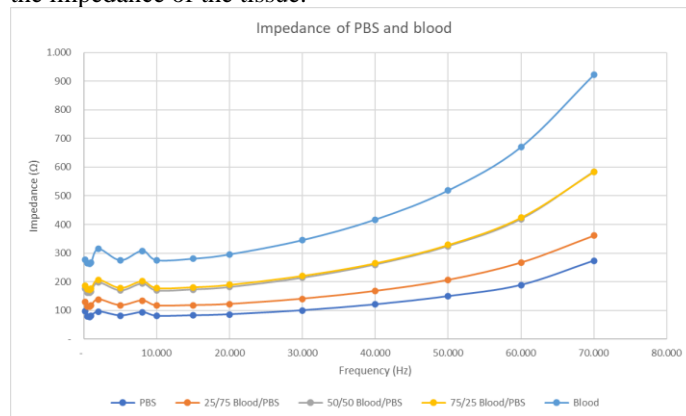

Figure 15. The impedance of PBS and blood mixtures. The red blood cells behave like a combination of cell membranes and intracellular fluid while the PBS behaves like extracellular fluid.

A. Results through the artery, what went wrong?

The striking difference between the results of the measurements through the artery and on the kidney is the range in which these values differ. The changes in impedance for the high frequency signal through the artery occur around the 70.000 Ω while the changes on the kidney for the same signal occur at the 0 to 900 Ω range. The results through the artery all show similar behaviour. The results of the on the kidney measurements do not. It is therefore important to discuss the through the artery measurements first before delving deeper into the on the kidney results per experiment set.

The results through the artery display almost no differences between the half of the porcine kidney that was the focus of the experiment and the control half as can be seen in **Figure 16**. All the graphs of the measurements through the artery data be found in **Appendix 2, 3,** and **5**.
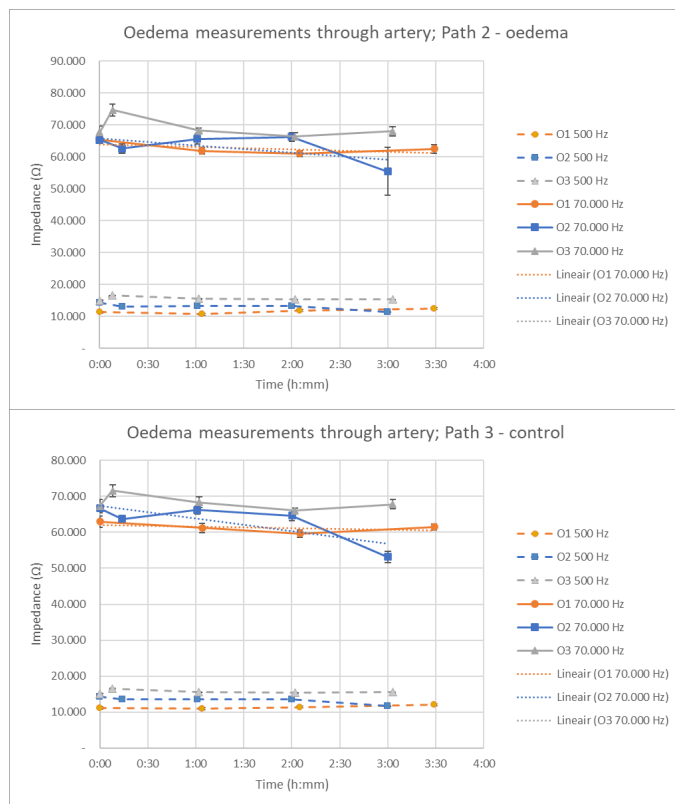

Figure 16. *Results of the oedema measurements through the renal artery.*

Not one result demonstrated the behaviour of the predictive models. A possible explanation for this can be that components of the system that is set up to do the measurements through the artery create more impedance change than are measured by the modifications to the kidney. Although the standard deviation of the artery measurements is small compared to the measurements itself, it is still larger than the complete range of the changes in impedance measurement on the kidney (> 1.000 Ω). An examination of multiple variables was conducted after these results emerged. A pressure difference did not change the impedance, the accompanying graph is shown in **Figure 17**. The impedance of the perfusate was analysed before every measurement during D2 and D3. The

presence and amount of cellular tissue in the perfusate did not change the impedance of the perfusate, the graph and these data points can be found in **Figure 19** and **Appendix 8**. What did have an impact on the impedance was the length of the tubing used before entering the kidney (**Figure 17** and **Appendix 7**). The data that can be found in **Figure 17** demonstrates an increase of 250 Ω/cm at the low frequencies and an increase of 730 Ω/cm at the high frequencies. Other components that have a major impact on the impedance are the three-way valves used in the circuit as can be seen in **Figure 17**. The three-way valves between the two electrode pairs cause an impedance increase of approximately 7.000 Ω per valve at the low frequencies and an increase of 15.000 Ω per valve at the high frequencies. The standard deviation for the three-way valve impedances is 1.000 Ω at the low frequencies and 2.000 Ω at the high frequencies. More three-way valve data can be found in **Appendix 9**. The standard deviation for the valves alone is already greater than the ranges of impedance changes measured on the kidney. The results of the measurements through the artery can therefore not be used for a proper analysis. The setup for these measurements needs to be revised so that the components of the circuit do not interfere with the impedance measurements inside of the kidney.
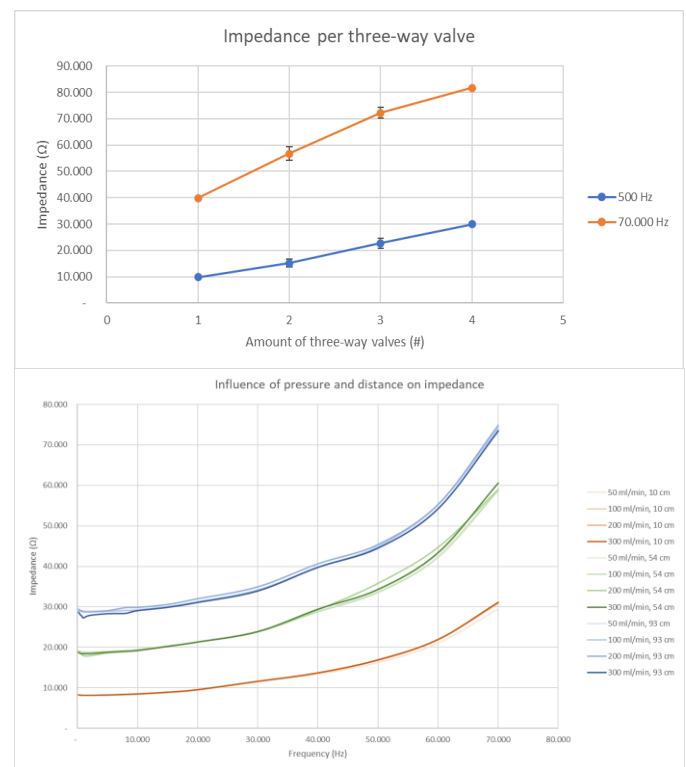
Figure 17. *Left: The impedance of three-way valves. The standard deviation is greater than the impedance changes measured on the kidney. Right: The influence of pressure through the system and distance through the tubing on impedance. Pressure has no influence on impedance but distance does.*

B. Decellularization results

Three decellularization experiments were conducted on porcine kidneys. These kidneys will be labelled as D1, D2 and D3 throughout the rest of this paper. All three of these kidneys have measurements through the artery while only D2 and D3

have measurements on the kidney. Faulty electrode placement on D1 caused some of the data to be unreliable, this data has been excluded from the results. An artery or vein could have been clogged during the decellularization process of D2, causing the kidney to become half decellularized and half partially decellularized as seen in **Figure 18**.
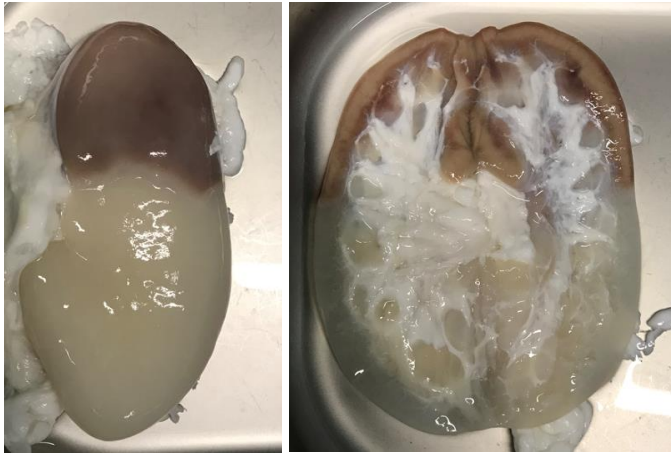

Figure 18. Left: Kidney D2, partially decellularized. Right: Kidney D2, sliced open.

The decellularization process results of the measurements on the kidney are shown Figure **19**. Larger images of the graphs can be found in **Appendix 2**. The dH2O measurements are not shown in the left figure because the low conductivity of the dH2O increased the impedance too much to observe the changes during the rest of the experiment as shown in the right figure. More data on the influence of the perfusate on the impedance can be The trend lines display the linear regression of the high frequency data during the decellularization process. The trendlines of both D2 and D3 show a decline. D2, the partially decellularized kidney, displays a smaller decrease in impedance during the decellularization process than D3. The biggest changes for D3 transpire on the first day. The trend lines of the lower frequencies display little variation compared to the trend lines of the higher frequencies and are therefore not depicted.

Measurements were taken of the decellularized and partially decellularized halves of D2 beginning 1 day and 18 hours after the experiment started. These measurements were taken as described in the Methods section on the experiment setup for measurements *on the kidney*. The measurements on the kidney can be seen in **Figure 20** and **Appendix 2**. The differences between the decellularized and partially decellularized halves should be seen as the differences between dead cells and the absence of cells as the kidney cells would not be alive anymore after 2 days. Both trendlines of the measurements on the kidneys show a decrease in impedance.
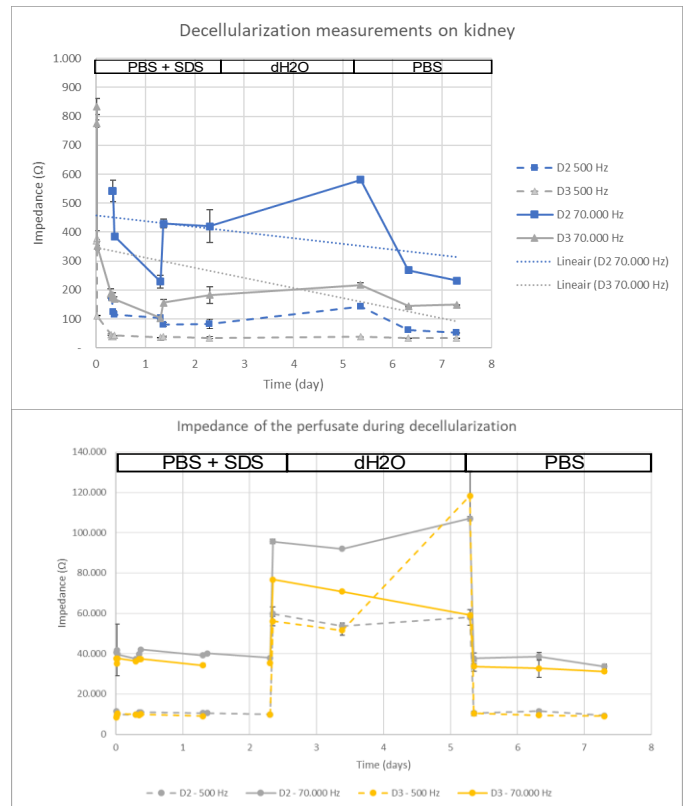

Figure 19. Left: Results of the decellularization process measurements on the kidney. Right: The influence of perfusate on the impedance. dH2O causes a spike in impedance
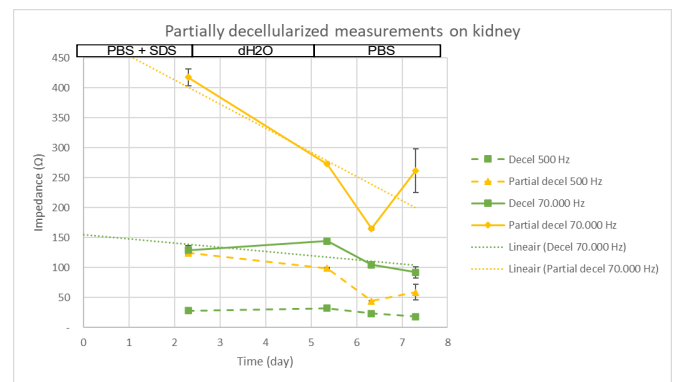
Figure 20. Results of the decellularized and partially decellularized halves of porcine kidney D2.

C. Oedema results

Three oedema experiments were conducted on porcine kidneys. These kidneys will be labelled as O1, O2 and O3 throughout the rest of this paper. A noticeable swelling occurred in all three kidneys on side of the kidney where the renal capsule was cut. The results of the oedema measurements on the kidney are not stable as seen in **Figure 22** and **Appendix 4**. The results for the whole kidney path did not show any noteworthy phenomenon and can be found in **Appendix 4**. Only O1 displays a stable impedance at the control side of the kidney. The higher and lower frequencies of O2 and O3 on the control side display large increases and decreases during the oedema formation process in an unpredictable manner. The

impedance of the low frequencies exceeds the high frequency impedance of O2 at the 15-minute mark on the oedema side. The impedance of both O2 and O3 show a sudden increase at the 3-hour mark on the oedema side of the kidney.

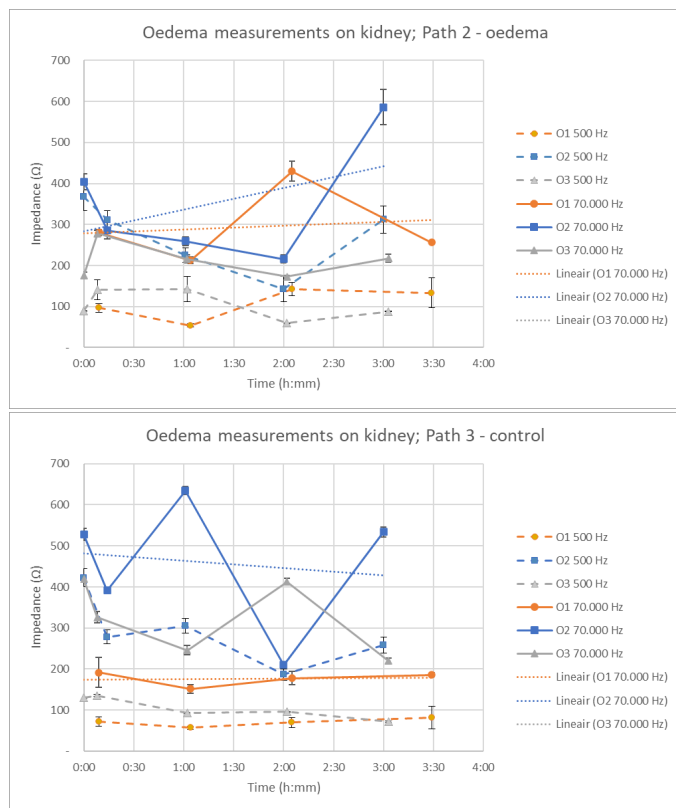Figure 21. Results of the vascular obstruction measurements on the kidney.

D. Vascular obstruction simulation results

Three vascular obstruction simulation experiments were conducted on porcine kidneys. These kidneys will be labelled as V1, V2 and V3 throughout the rest of this paper. These experiments had the vascular clamp applied after the first measurement and removed at the 1-hour mark. After the vascular clamp was applied, the control half of both V1 and V2 coloured blue while perfusing with methylene blue. The methylene blue through V3 produced more of a frontside and backside divide instead of an upper and lower half divide. The electrode placement was altered to accommodate for this difference.

Only the high frequency V2 data presents the expected increase in impedance on the blockade side after the appliance of the vascular clamp and decrease after removal as seen in **Figure 21** and **Appendix 6**. The control side of V3 shows an increase and decrease expected from the blockade side except for the last data point. The control measurements of both V2 and V3 exhibit less variability than the control measurements of the oedema experiment but are still not stable. The results for the whole kidney path did not show any noteworthy phenomenon and can be found in **Appendix 6**.
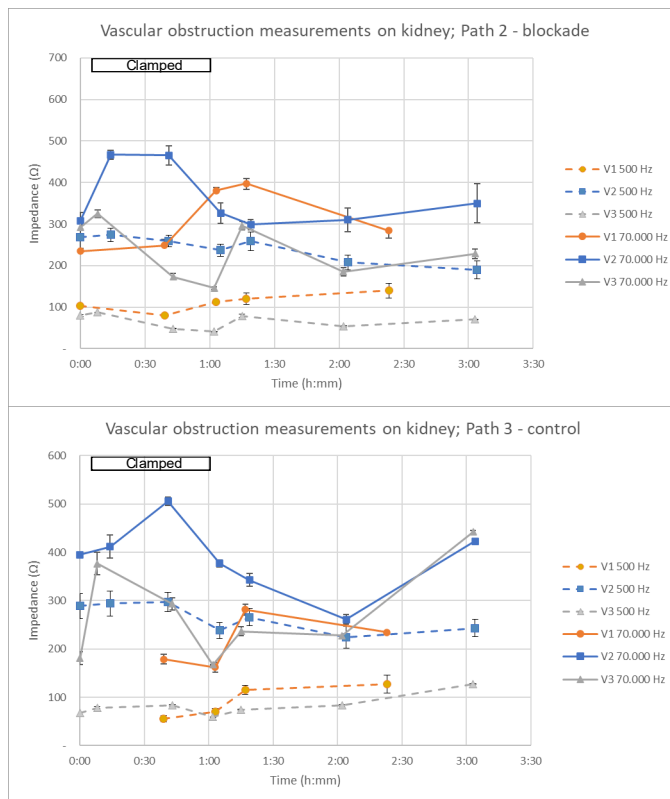

Figure 22. Results of the oedema measurements on the kidney.

IV. DISCUSSION

A. The decellularization process

The decellularization results of the measurements on the kidney show a decreasing trendline during the decellularization process (**Figure 19**) as was predicted by the model (**Figure 7**). Both D2 and D3 show an increase in impedance at day 5 of the experiment. This is the first data point after the dH2O flushing. This increase can be caused by residue dH2O in the cell tissue. D3 displays a significant drop in impedance on the first day of the process. The high frequency impedance values of D3 drop to the low frequency range. The low frequency impedance of D3 starts to approach the impedance of PBS as can be found in **Figure 15**. The high frequency signal of D2 exhibits a same drop in impedance to a lesser extent on the first day as D3 but increases again on day 2. The cause of this sudden increase is unknown but can be due to a change in electrode placement or the blocking of an artery or vein. This is also the moment that the kidney showed indications of partial decellularization. The differences that can be observed between the partial and fully decellularized halves of D2 as seen in **Figure 20** show that the decellularized half of the kidney displayed a high frequency impedance that is on par with the values for low frequency impedance and a low frequency impedance that approximated the impedance of PBS. The decline of the partial decellularized side of D2 could be caused by the further deterioration of the dead cells present in that half.

B. Oedema formation

The data of the oedema formation is unstable. The expected stable line on the control side of the porcine kidney is only visible at O1 as seen in **Figure 22**. However, this is the only kidney that didn't display anything close to the predictions (**Figure 11**) of the impedance changes during oedema formation. Both the high frequencies of O1 and O2 indicate the decreasing impedance during oedema formation until the 3-hour mark. There is no clear explanation for this outlier visible on the control side of O2 and O3. The low frequency signals on the oedema half of the kidneys seem to experience more changes than their counterparts on the control side. Yet, these changes don't follow the predicted path. The low and high frequency signals are too erratic to determine a clear correlation between impedance and oedema formation.

C. Vascular obstruction simulation

The vascular obstruction simulation displays less erratic results in the control group. Although, the control data is not the stable line that is to be expected. Most notably, the high frequency signal of the V3 control side depicts the behaviour expected of the blockade side (**Figure 21**). An increase in impedance after application of the clamp followed by a decrease in impedance upon resealing the clamp after the 1-hour mark as predicted in **Figure 13**. This could be caused by the unusual anatomy of V3 compared to V1 and V2. The two branches of the renal artery of V3 supply the front and back half of the kidney instead of the upper and lower halves as with V1 and V2. The altered electrode placement could have been faulty. The only other signal that expresses the expected behaviour is the high frequency signal of the blockade side of V2. However, the control signal of V2 is not stable enough to come to definitive conclusions. Noteworthy is that the blockade doesn't seem to influence the low frequency signals. The low frequency signals of the blockade and control halves are almost interchangeable.

D. Limitations of the study

There are a few limitations to the study. Firstly, there is a technique to calculate resistance and reactance from the impedance [15], [17], [18]. The resistance represents the influence of the extracellular fluid and the reactance the influence of the cell membrane capacitance in combination with the intracellular fluid. This technique needs the voltage and current values and the phase shift between the sending and receiving sinusoidal signals to calculate these resistance and reactance [15], [17], [18]. The Spectra Impedance kit has the components to retrieve the phase shift, voltage and current values but reprogramming the equipment could not be completed during the scope of this research [28]. There are too many unknown variables in **equation 4, 5 and 10** to determine the exact values for the extracellular resistance, the cell membrane capacitance, and the intracellular resistance or an estimation without this technique. The impedance changes of the EIS are now interpreted as changes in tissue composition but this technique would better substantiate that interpretation. The use of this technique could give more insight into the inner workings of the kidney tissue and could define impedance more precisely.

The second limitation is that the maximum frequency of the Spectra Bioimpedance kit is 70.000 Hz. A frequency of >5 MHz would be needed to best represent the impedance of intra- and extracellular fluid combined [17]. This would also influence the penetration depth and decrease it to less than 7,5 mm [26]. A higher frequency with a penetration depth above the length of the kidney (approximately 16 cm) is needed to lessen the unpredictable interference of the cell membrane capacitance.

Thirdly, the EIS was used for the experiments while EIT could give a better representation. The signal between 32 electrodes could then be used to visualize the inside of the kidney instead of the signal between 4 electrodes. This plurality of data could also mean that errors are more likely to be noticed. The Graz Consensus algorithm displays the data in an easy to understand an intuitive manner and EIT is therefore easier to implement in an medical setting then EIS where the user needs to understand what the different values represent and what values are odd and normal.

Fourthly, the placement of electrodes was done by hand. The Spectra Bioimpedance kit had four electrodes available for EIS. All these electrodes were needed for every measurement during the experiments. Six different paths at every timestamp caused a lot of movement of the electrodes. This in combination with multiple experiments at the same time resulted in even more electrode movement. Some of the results may be influenced by the electrode placement or misplacement. The influence of electrode placement was evaluated by providing data on impedance per distance through the cortex and medulla of the porcine kidney. This data can be found in **Appendix 11**. It revealed an impedance increase of approximately 8 Ω/mm through the medulla and 10 Ω/mm through the cortex. Ideally, the electrodes should be placed at exactly the same place on the kidney throughout the experiment without being moved to prevent variability in impedance due to electrode placement. This could be achieved by a container in which the electrodes would be fixed.

The fifth limitation is that the vascular obstruction and oedema experiments use DMEM/F-12 cell culture medium for perfusion. Experiments with kidneys that need more oxygen often use blood for the extra oxygen carriers. Blood has the same three-element equivalent circuit as the kidney tissue, where the red blood cells replace the cell membrane capacitance and intracellular fluid and the blood plasma replaces the extracellular fluid [27]. Tests have been performed to establish the impedance of blood at different frequencies. The results of these tests can be found in **Appendix 10**. Normal blood has an impedance of 900 Ω at high frequencies and can therefore influence the EIS results notably, especially the results of the measurements through the artery.

Sixthly, the flow through the organs variated a lot between the different kidneys and sometimes even between two

measurements in the same kidney. The flow was sensor-controlled by adjusting the pressure. These variable pressures and flow could damage or alter the inside anatomy of the kidney and influence the impedance change. At best, only kidneys with the same pressure to reach the same flow would be used as comparisons.

Lastly, the study is done on porcine kidneys. The end goal is the medical application of the EIS technique on human kidneys. The porcine kidney is used as a replacement for this exploratory research because of the close analogies between structural features of the human and porcine kidney [29]. As Giraud et al. describe "Although pig renal and intrarenal anatomy could not be completely transposed to human, many similarities in porcine and human intrarenal arteries have been described as well as anatomical relationships between intrarenal arteries and the kidney collecting system" [29]. Even though the porcine kidneys serve as a good replacement for human kidneys in the exploratory phase of electrical impedance spectroscopy, later research needs to take into account that the human kidney can react in a completely different way. This could for instance be caused by the notable size difference of the kidneys.

E. Recommendations

To advance the field, research could be done to establish what setup doesn't interfere with data collection for the measurements through the artery. The results of the experiments through the artery were not usable. The theory behind this measurement technique can't be proven or disproven by the results because the interference stems from the circuit before entering the kidney.

Further research could be done to establish a clear connection between impedance and decellularization quality. The data suggests that the impedance will not decrease anymore after the second day. Further research could be done to establish if these results can help in accelerating the decellularization process. The porcine kidney D2 is partially decellularized by accident but further research could be done in a more controlled environment to test the differences between decellularized and dead tissue to further control and monitor the decellularization process in a non-invasive manner.

Additional oedema research needs to be done to determine if a correlation between oedema formation and impedance exists. This research could benefit from more measurements during the 3 hour perfusion period and to be repeated more often. This was not possible during this research because multiple experiments were conducted at the same time. This would show a gradual change in impedance instead of the erratic changes that are visible now, as seen on the control sides of O2 and O3. Further research could also benefit from a tissue analysis after the experiment to establish the impact of the oedema on the kidney.

Supplementary vascular obstruction research has to be done to establish if the reaction of V2 is the norm or just an outlier. Follow-up research needs to do this experiment in greater numbers and with more data points in the 3-hour span. Further research could also be done on the effects of different clamping times and the amount of cell death after a blockade that lasted for a longer period. Further research could also benefit from a tissue analysis after the experiment to establish the damage done by the blockade.

Future research should also examine the impedance of higher frequency signals and study the resistance and reactance that can be obtained from measuring the impedance and the phase shift. These additional explorations in impedance change could add a new layer of depth and understanding to the inner workings of the kidneys.

Eventually, research needs to be done on human kidneys, possibly with blood instead of the cell culture medium, to validate the EIS technique for medical use in the transplantation department. Both these adjustments could have a major impact on the impedance behaviour as can be seen with the difference in impedance for blood and PBS in **Figure 15**. It is therefore important that extensive research is completed before implementation on human subjects.

V. Conclusion

The research question of this paper is: "*Is it possible to detect vascular obstructions and oedemas or monitor the decellularization process in perfused ex-vivo porcine kidneys using electrical impedance spectroscopy?*". Three different models and two different measuring methods were tested to determine if this was possible. Robust changes have been made to the porcine kidneys in this regard. The set-up of the measurements through the artery had too much interference for the data to be usable. The changes in impedance during the measurements on the kidney did not show the significant changes that were expected. The sensitivity of the methods is less than expected. The changes in impedance seem subtle. Only the decellularization results showed a notable change over time. The conclusion of this research is therefore: The results cannot prove a clear connection between vascular obstruction and oedema detection and electrical impedance changes. There is a probable correlation between electrical impedance and the phase of decellularization in which the kidney is in. Follow-up research is needed to substantiate this further.

.

VI. References

[1] A. S. Levey and J. Coresh, 'Chronic kidney disease', *Lancet Lond. Engl.*, vol. 379, no. 9811, pp. 165–180, Jan. 2012, doi: 10.1016/S0140-6736(11)60178-5.

[2] Nierstichting, 'Feiten en cijfers', *Nierstichting*, 2022. https://nierstichting.nl/leven-met-een-nierziekte/feiten-en-cijfers/ (accessed Jan. 11, 2022).

[3] M. B. F. Pool, T. L. Hamelink, H. van Goor, M. C. van den Heuvel, H. G. D. Leuvenink, and C. Moers, 'Prolonged ex-vivo normothermic kidney perfusion: The impact of perfusate composition', *PLOS ONE*, vol. 16, no. 5, p. e0251595, May 2021, doi: 10.1371/journal.pone.0251595.

[4] T. R. Elliott, M. L. Nicholson, and S. A. Hosgood, 'Normothermic kidney perfusion: An overview of protocols and strategies', *Am. J. Transplant.*, vol. 21, no. 4, pp. 1382–1390, 2021, doi: 10.1111/ajt.16307.

[5] KDPI, 'KDPI Calculator - OPTN', 2021. https://optn.transplant.hrsa.gov/resources/allocation-calculators/kdpi-calculator/

[6] KDPI, 'A Guide to Calculating and Interpreting the Kidney Donor Profile Index', 2021. https://optn.transplant.hrsa.gov/media/4615/kdpi_guide.pdf

[7] S. A. Hosgood, E. Thompson, T. Moore, C. H. Wilson, and M. L. Nicholson, 'Normothermic machine perfusion for the assessment and transplantation of declined human kidneys from donation after circulatory death donors', *Br. J. Surg.*, vol. 105, no. 4, pp. 388–394, Mar. 2018, doi: 10.1002/bjs.10733.

[8] T. Prudhomme *et al.*, 'Ischemia-Reperfusion Injuries Assessment during Pancreas Preservation', *Int. J. Mol. Sci.*, vol. 22, no. 10, p. 5172, May 2021, doi: 10.3390/ijms22105172.

[9] T. E. Kerner, K. D. Paulsen, A. Hartov, S. K. Soho, and S. P. Poplack, 'Electrical impedance spectroscopy of the breast: clinical imaging results in 26 subjects', *IEEE Trans. Med. Imaging*, vol. 21, no. 6, pp. 638–645, Jun. 2002, doi: 10.1109/TMI.2002.800606.

[10] D. G. Leuning *et al.*, 'Vascular bioengineering of scaffolds derived from human discarded transplant kidneys using human pluripotent stem cell–derived endothelium', *Am. J. Transplant.*, vol. 19, no. 5, pp. 1328–1343, May 2019, doi: 10.1111/ajt.15200.

[11] T. K. Bera and N. Jampana, 'Electrical Impedance Spectroscopic Study of Broiler Chicken Tissues Suitable for The Development of Practical Phantoms in Multifrequency EIT', *J. Electr. Bioimpedance*, vol. 2, pp. 48–63, Mar. 2011, doi: 10.5617/jeb.174.

[12] C.-A. González-Correa, 'Clinical Applications of Electrical Impedance Spectroscopy', in *Bioimpedance in Biomedical Applications and Research*, F. Simini and P. Bertemes-Filho, Eds. Cham: Springer International Publishing, 2018, pp. 187–218. doi: 10.1007/978-3-319-74388-2_10.

[13] T. K. Bera, J. Nagaraju, and G. Lubineau, 'Electrical impedance spectroscopy (EIS)-based evaluation of biological tissue phantoms to study multifrequency electrical impedance tomography (Mf-EIT) systems', *J. Vis.*, vol. 19, no. 4, pp. 691–713, Nov. 2016, doi: 10.1007/s12650-016-0351-0.

[14] J. Estrela da Silva, J. P. Marques de Sá, and J. Jossinet, 'Classification of breast tissue by electrical impedance spectroscopy', *Med. Biol. Eng. Comput.*, vol. 38, no. 1, pp. 26–30, Jan. 2000, doi: 10.1007/BF02344684.

[15] S. F. Khalil, M. S. Mohktar, and F. Ibrahim, 'The Theory and Fundamentals of Bioimpedance Analysis in Clinical Status Monitoring and Diagnosis of Diseases', *Sensors*, vol. 14, no. 6, pp. 10895–10928, Jun. 2014, doi: 10.3390/s140610895.

[16] T. K. Bera, 'Bioelectrical Impedance Methods for Noninvasive Health Monitoring: A Review', *J. Med. Eng.*, vol. 2014, pp. 1–28, Jun. 2014, doi: 10.1155/2014/381251.

[17] M. Y. Jaffrin and H. Morel, 'Body fluid volumes measurements by impedance: A review of bioimpedance spectroscopy (BIS) and bioimpedance analysis (BIA) methods', *Med. Eng. Phys.*, vol. 30, no. 10, pp. 1257–1269, Dec. 2008, doi: 10.1016/j.medengphy.2008.06.009.

[18] GAMRY, 'Basics of EIS: Electrochemical Research-Impedance', 2022. https://www.gamry.com/application-notes/EIS/basics-of-electrochemical-impedance-spectroscopy/ (accessed Jan. 11, 2022).

[19] M. Lacey, 'Simple circuits with resistors and capacitors', *Matt Lacey*, Jan. 11, 2022. http://lacey.se/science/eis/simple-circuits/ (accessed Jan. 11, 2022).

[20] R. Petibon, 'STUDY OF ELECTROLYTE ADDITIVES IN LI-ION BATTERIES USING ELECTROCHEMICAL IMPEDANCE SPECTROSCOPY ON SYMMETRIC CELLS', p. 164.

[21] Mindseye Biomedical, 'Spectra Bioimpedance and EIT Complete Kit', *Mindseye Biomedical*, 2022. https://mindseyebiomedical.com/products/spectra-deluxe-kit (accessed Jan. 11, 2022).

[22] M. J. A. de Haan, F. M. R. Witjas, M. A. Engelse, and T. J. Rabelink, 'Have we hit a wall with whole kidney decellularization and recellularization: A review', *Curr. Opin. Biomed. Eng.*, vol. 20, p. 100335, Dec. 2021, doi: 10.1016/j.cobme.2021.100335.

[23] J. J. Song, J. P. Guyette, S. E. Gilpin, G. Gonzalez, J. P. Vacanti, and H. C. Ott, 'Regeneration and experimental orthotopic transplantation of a bioengineered kidney', *Nat. Med.*, vol. 19, no. 5, pp. 646–651, May 2013, doi: 10.1038/nm.3154.

[24] A. Kataria, S. Magoon, B. Makkar, and A. Gundroo, 'Machine perfusion in kidney transplantation', *Curr. Opin. Organ Transplant.*, vol. 24, no. 4, pp. 378–384, Aug. 2019, doi: 10.1097/MOT.0000000000000675.

[25] T. E. of E. Britannica, 'renal capsule', *Encyclopedia Britannica*, Nov. 12, 2018. https://www.britannica.com/science/renal-capsule (accessed Jan. 11, 2022).

[26] IFAC, 'Dielectric Properties of Body Tissues: Output data', 2022. http://niremf.ifac.cnr.it/tissprop/htmlclie/uniquery.php?func=stsffun&tiss=Kidney&freq=70000&outform=disphtm&tisname=on&frequen=on&conduct=on&permitt=on&losstan=on&wavelen=on&pendept=on&freq1=1000000&tissue2=Kidney&frqbeg=500&frqend=70000&linstep=100&mode=log&logstep=5&tissue3=Kidney&freq3=70000 (accessed Jan. 11, 2022).

[27] Z. Chang, G. Pop, and G. Meijer, 'A Comparison of Two- and Four-Electrode Techniques to Characterize Blood Impedance for the Frequency Range of 100 Hz to 100 MHz', *IEEE Trans. Biomed. Eng.*, vol. 55, pp. 1247–9, Apr. 2008, doi: 10.1109/TBME.2008.915725.

[28] J. Rintoul, *EIT_Firmware/OpenEIT.c*. Open EIT, 2021. Accessed: Jan. 11, 2022. [Online]. Available: https://github.com/OpenEIT/EIT_Firmware/blob/38a181367ba83a05442d6fc695213be0d3f29f9f/OpenEIT.c

[29] S. Giraud, F. Favreau, N. Chatauret, R. Thuillier, S. Maiga, and T. Hauet, 'Contribution of Large Pig for Renal Ischemia-Reperfusion and Transplantation Studies: The Preclinical Model', *J. Biomed. Biotechnol.*, vol. 2011, pp. 1–14, 2011, doi: 10.1155/2011/532127.

[30] S. W. Smith, 'CHAPTER 25 - Special Imaging Techniques', in *Digital Signal Processing*, S. W. Smith, Ed. Boston: Newnes, 2003, pp. 423–450. doi: 10.1016/B978-0-7506-7444-7/50062-5.

[31] A. Adler *et al.*, 'GREIT: a unified approach to 2D linear EIT reconstruction of lung images', *Physiol. Meas.*, vol. 30, no. 6, pp. S35–S55, Jun. 2009, doi: 10.1088/0967-3334/30/6/S03.

[32] C. N. Pai, J. Aya, and R. Lima, 'An implementation of the back-projection algorithm according to santosa and vogelius', *ABCM Symp. Ser. Bioeng.*, vol. 1, Jan. 2006.

[33] D. Constales, G. S. Yablonsky, D. R. D'hooge, J. W. Thybaut, and G. B. Marin, 'Chapter 9 - Experimental Data Analysis: Data Processing and Regression', in *Advanced Data Analysis & Modelling in Chemical Engineering*, D. Constales, G. S. Yablonsky, D. R. D'hooge, J. W. Thybaut, and G. B. Marin, Eds. Amsterdam: Elsevier, 2017, pp. 285–306. doi: 10.1016/B978-0-444-59485-3.00009-6.

[34] A. Widodo and E. Endarko, 'Experimental study of one step linear Gauss-Newton algorithm for improving the quality of image reconstruction in high-speed Electrical Impedance Tomography (EIT)', *J. Phys. Conf. Ser.*, vol. 1120, p. 012067, Nov. 2018, doi: 10.1088/1742-6596/1120/1/012067.

Appendix 1- Electrical impedance tomography algorithms

The three algorithms that can be used by the EIT kit are the Back Projection, the Gauss-Newton Method, and the Graz Consensus.

Back Projection

Back projection views a medium from different angles and then combines these angles into one image as seen in figure 5. The image from a normal back projection is blurry. By filtering the signal before applying the back projection the blurring is corrected in the final image [30]. The Sheffield back projection is used for CT scans but this model is lacking for EIT because of the difference of X-ray and electric current propagation [31]. The Sheffield back projection assumes that the region between two adjacent potential lines has an equal voltage [32]. The different angles are established by rotating the current injection position as seen in figure 6. The Sheffield Mark I algorithm was developed especially for EIT applications. However, the formulation of this algorithm has been lost. Adler et al. calculated the linear-least square solution to $\mathbf{YR}_{SBP} = \mathbf{X}$ where $\mathbf{Y}$ is a matrix formed of datasets and $\mathbf{X}$ is a matrix formed of the associated reconstructed images that they got from a Sheffield Mark I device [31]. Adler et al. use this this version of the back projection for their parameter testing.
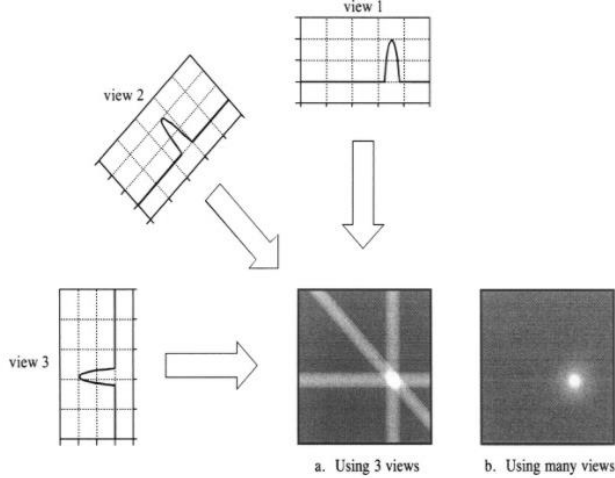

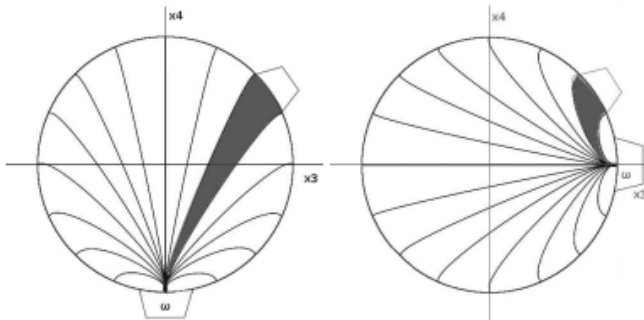**Figure 5.** Combining different views to create one image using the back projection [30]

Figure 6. Each coloured region has one current value according to the Sheffield back projection [32]

Gauss-Newton method

The Gauss-Newton method is an iterative algorithm that uses an educated guess as initial starting values for parameters and finds the best approximation of the values for these parameters by minimizing the sum of squares [33]. The following equation is used to estimate a next iteration[33]:

$$f(\mathbf{b_0} + \Delta\mathbf{b}) \approx f(\mathbf{b_0}) + \mathbf{J_0} * \Delta\mathbf{b}$$

(eq. 1)

With $\mathbf{b_0}$ the starting point, $\Delta\mathbf{b}$ the step size, and $\mathbf{J_0}$ the Jaccobian. When substituting $f(\mathbf{b_0} + \Delta\mathbf{b})$ for $\mathbf{y}$, the equation can be rewrite as:

$$\mathbf{J_0} * \Delta\mathbf{b} = \mathbf{y} - f(\mathbf{b_0})$$

(eq. 2)

This equation has the same structure as a $\mathbf{Ax} = \mathbf{b}$ equation an can be approximated using the linear least square method which gives the Gauss-Newton equation:

$$\Delta\mathbf{b} = \left(\mathbf{J_0^T J_0}\right)^{-1} \mathbf{J_0^T}(\mathbf{y} - f(\mathbf{b_0}))$$

(eq. 3)

However, for EIT a one-step linear Gauss-Newton is used to allow for rapid, real time imaging [31]. A mesh must be created using the Finite Element Method (FEM) before the one step linear Gauss-Newton can be run as shown in figure 7 [34]. The FEM creates a mesh of nodal elements that each represent one value of conductivity.
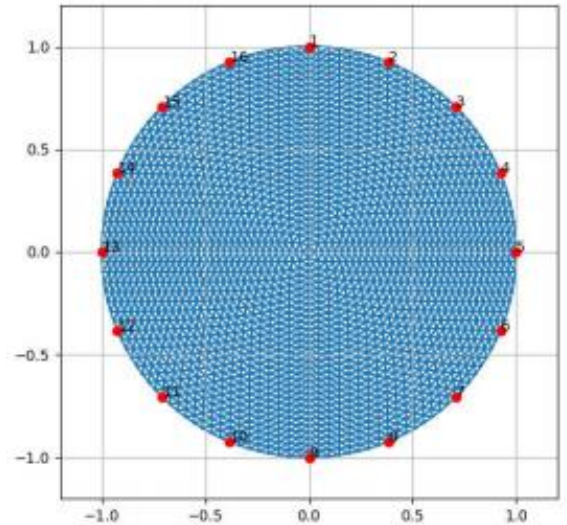

Figure 7. Finite element method of the circular container [34]

Next, the mathematical model of the one step linear Gauss-Newton can be run [10]. The mathematical formula for the one step linear Gauss-Newton is:

$$\hat{\mathbf{x}} = (\mathbf{J^T V^{-1} J} + \lambda^2 \mathbf{P^{-1}})^{-1} \mathbf{J^T V^{-1} y}$$

(eq. 4)

16

This is an generalised least squares solution to equation 1 with $\mathbf{V}$ the measurement accuracy, and the added parameters of an regularization hyperparameter λ and a regularization matrix $\mathbf{P}$. The regularization matrix models the likelihood of the image elements and their interactions and the regularization hyperparameter controls the trade-off between resolution and noise attenuation in the reconstructed image [31]. The study of Widodo et al. [34] shows that these parameters can be changed and finetuned to get a reconstructed image that closely fits the real image. Adler et al. [31] rewrite this formula to a less computational form that improves invers accuracy and stability:

$$\mathbf{R_{GN}} = \mathbf{PJ}^T(\mathbf{JP\,J}^T + \lambda^2\mathbf{V})^{-1}$$

(eq. 5)

This is the final version of the one-step Gauss-Newton algorithm that was used in the tests of Adler et al. for the parameter testing.

Graz Consensus

The Graz Consensus reconstruction algorithm was developed to address the issue that the algorithms available for EIT were outdated and did not incorporate the advances made in the last 20 years [31]. The Graz Consensus is based on a forward model, a noise model and desired performance metrics. The FEM is used as a forward model to define the current state of the system and show the spatial reconstruction of the image [31]. The noise model used for the Graz Consensus considers electronic measurement noise, and electrode movement artefacts. The electronic measurement noise is modelled to be uniform and Gaussian [31]. The electrode movement artefacts are implemented in the study of Adler et al. by deforming the FEM but can also be based on a calibration protocol [31]. The desired measurement are achieved by creating a set of desired images, $\tilde{\mathbf{x}}_t$. The desired image are larger than the training inputs to achieve a more uniform resolution as seen in figure 8 [31].

Figure 8. The training inputs and desired output for target data and noise data [31]

An image weighting $\mathbf{w}^{(k)}$ represents the weight each pixel has in $\tilde{\mathbf{x}}_t$ and allows for tuning of the relative importance of metrics as shown in figure 9 [31]. There is an inner circular zone for each reconstructed image that needs to be flat to meet the AR and PE performance metrics [31]. Outside of the boundary

is another zone that needs to be zero to meet the RNG and SD performance metrics. In these zone $\mathbf{w}^{(k)}$ is large to give a substantial penalty to images that are not well tuned to the AR, PE, RNG and SD performance metrics. $\mathbf{w}^{(k)}$ is small in the transition zone for flexibility [31]. This is shown in figure 9 by the size of the error bars.
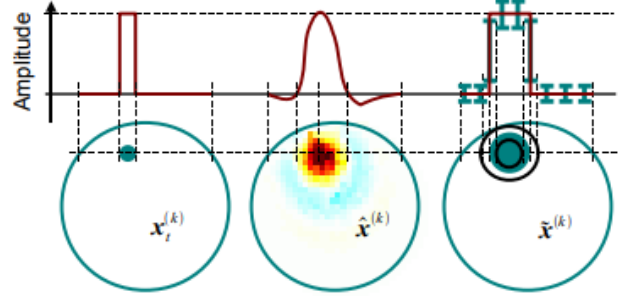
Figure 9. Implementation of the weighting. The error bars show how the weighting effects each pixel. The inner and outer circle have a high weighting and low error bars while the transition zone has a low weighting and thus large error bars [31]

Additionally, noise training data $\mathbf{y}_n$ is generated with the desired image $\tilde{\mathbf{x}}_n = \mathbf{0}$ as the noise input should produce no output as seen in figure 8. The same weighting $\mathbf{w}^{(k)}$ is used to control the pixels in this image. A large value for $\mathbf{w}^{(k)}$ results in a large penalty for image noise and a low NAMP parameter.

Adler et al. derive in their paper that the reconstruction matrix $\mathbf{R_{GC}}$ of the Graz Consensus minimizes the norm:

$$\left\| \left[\, \tilde{\mathbf{X}}_t | 0 \right] - \mathbf{R}[\mathbf{Y}_t | \mathbf{Y}_n] \right\|_{\mathbf{W}}^2$$

(eq. 6)

Where $\tilde{\mathbf{X}}_t$ is a matrix containing all the desired images, $\mathbf{Y}_t$ is a matrix containing all the training data, $\mathbf{Y}_n$ is a matrix containing all the noise training data, $\mathbf{W}$ is a matrix containing all the pixel weights. The operation [.|.] joins the two submatrices horizontally into one matrix [31]. Calculating the minimum norm offers the following equation:

$$\mathbf{R} = \tilde{\mathbf{X}}_t \mathbf{Y}_t^T (\mathbf{Y}_t\,\mathbf{Y}_t^T + \mathbf{Y}_n\,\mathbf{Y}_n^T)^{-1}$$

(eq. 7)

Adler et al. state that samples for $\mathbf{Y}_t$ may be approximated from the Jacobian when assuming the body is linear for small targets [31] and change the equation to:

$$\mathbf{R} = \tilde{\mathbf{X}}_t \mathbf{Y}_t^T (\mathbf{J}\Sigma_x \mathbf{J}^T + \Sigma_n)^{-1}$$

(eq. 8)

This is the equation that is used for testing parameter performance of the algorithm.

Parameter scores

Adler at al tested the three algorithms by reconstructing the images with identical data and reporting on how each

algorithm scored on each parameter [31]. The data was collected by placing a target in a circular container that was filled with water and had electrodes evenly spaced and submerged at the boundary of the container. This setup is described in more detail in the Method section of this paper. All the algorithms showed the same and uniform results when the target was positioned in the centre of the medium but behaved differently when the boundary of the medium was approached. **Table 1** shows the behaviour of each parameter when approaching the boundary.
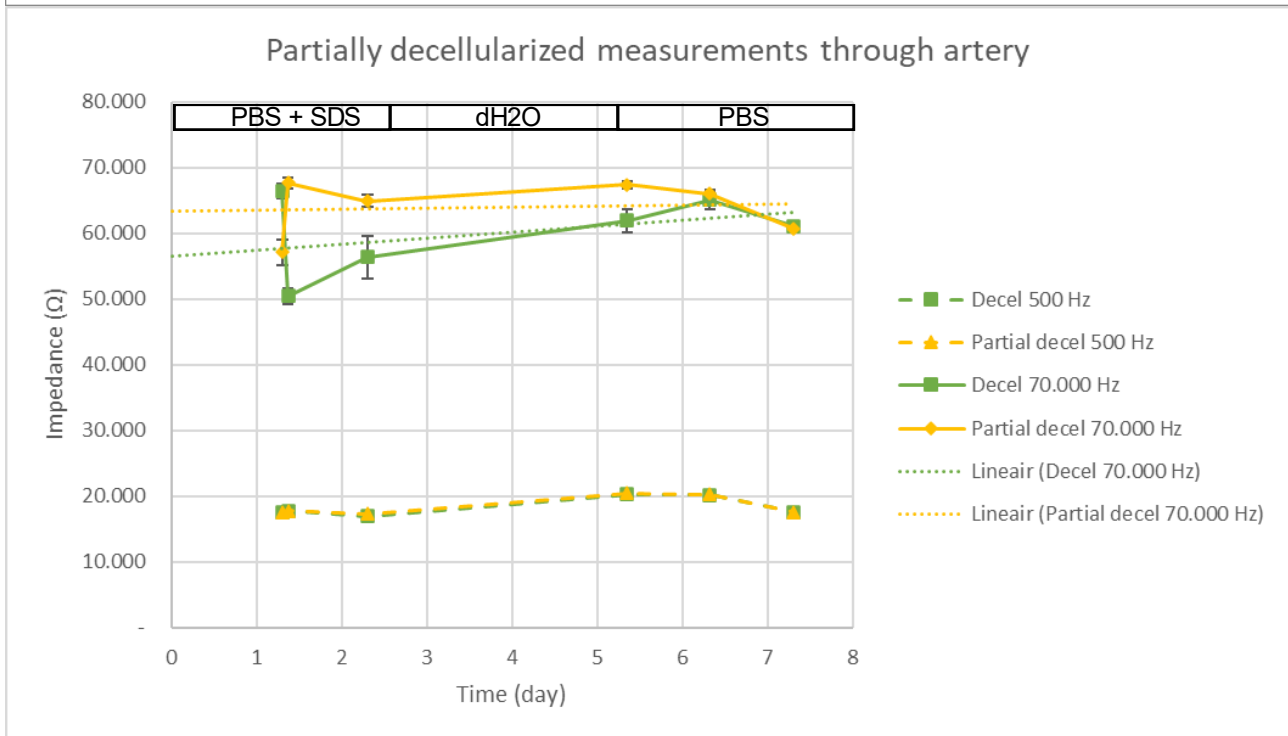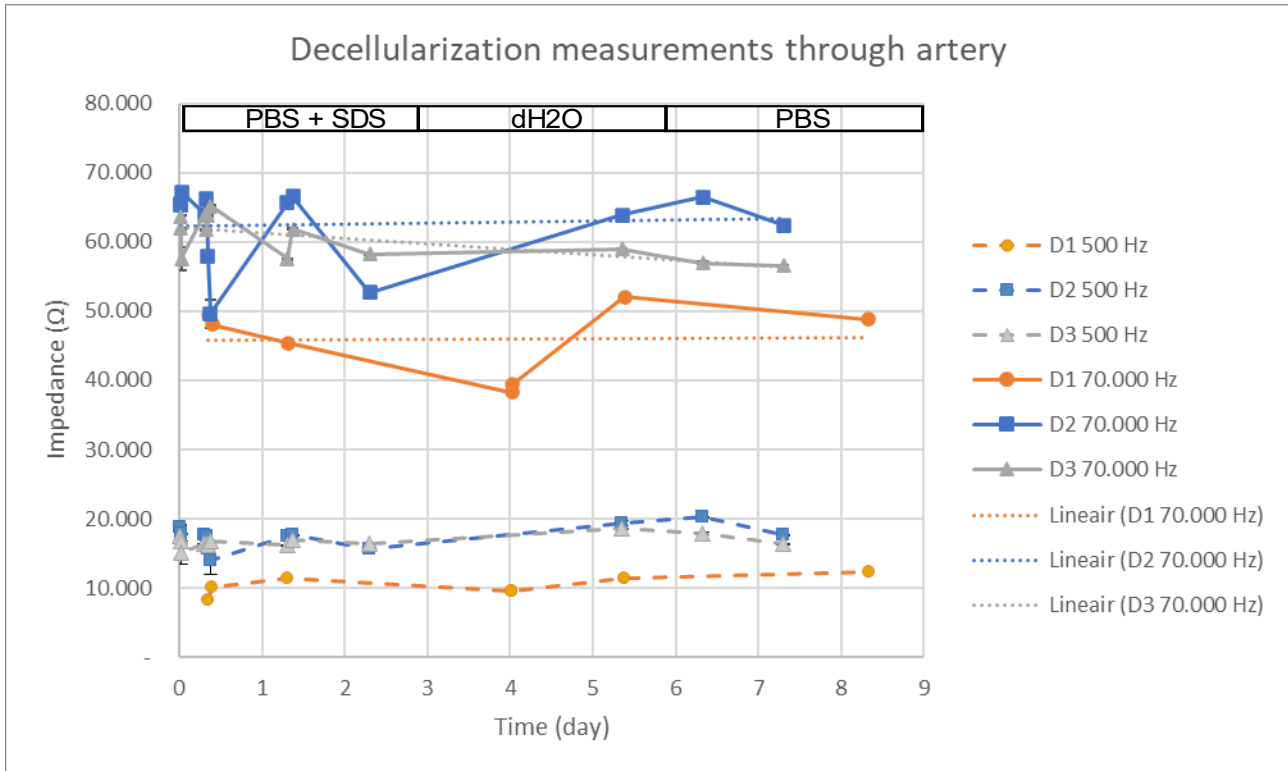
Choosing an algorithm

The Back Projection scores worst on all the parameters. The algorithm is unstable and highly variable near the boundary of the medium. The Gaus-Newton is a good algorithm for EIT but scores badly on the RNG parameter resulting in a false negative circle around the target and this can be interpreted as oedema when it is not present in the kidney. The Graz Consensus shows the behaviour that is the closest to the ideal behaviour for every parameter of the three algorithms. It is also the only algorithm that takes the NAMP parameter into account within the math of the algorithm itself. The Graz Consensus will therefore be the algorithm that will be used to assess oedema and blood clot forming in kidneys.

Parameter	Ideal behaviour	Back projection	Gauss-Newton	Graz Consensus
Amplitude response	Constant	Unstable	Decreases with higher variability near the boundary	Constant with higher variability near the boundary
Position error	Small with little variability	Becomes negative and then increases exponentially in the positive direction near the boundary	Stable and nearing 0 with higher variability near the boundary	Stable and nearing 0
Resolution	Uniform and small value	Increasing variability near the boundary	Uniform and small value	Uniform and small value
Shape deformation	Uniform and small value	Increases exponentially near the boundary	Uniform and small value	Uniform and small value
Ringing	Uniform and small value	Increases exponentially near the boundary	Increases exponentially near the boundary	Constant with higher variability near the boundary
Noise Amplification	Small value	Not taken into account in the algorithm	Not taken into account in the algorithm	Use of pixel weighting and noise training date as counteracting measures

Table 1. Parameter behaviour of each algorithm when approaching the boundary of the medium

Decellularization measurements through artery

Partially decellularized measurements through artery

Decellularization measurements on kidney
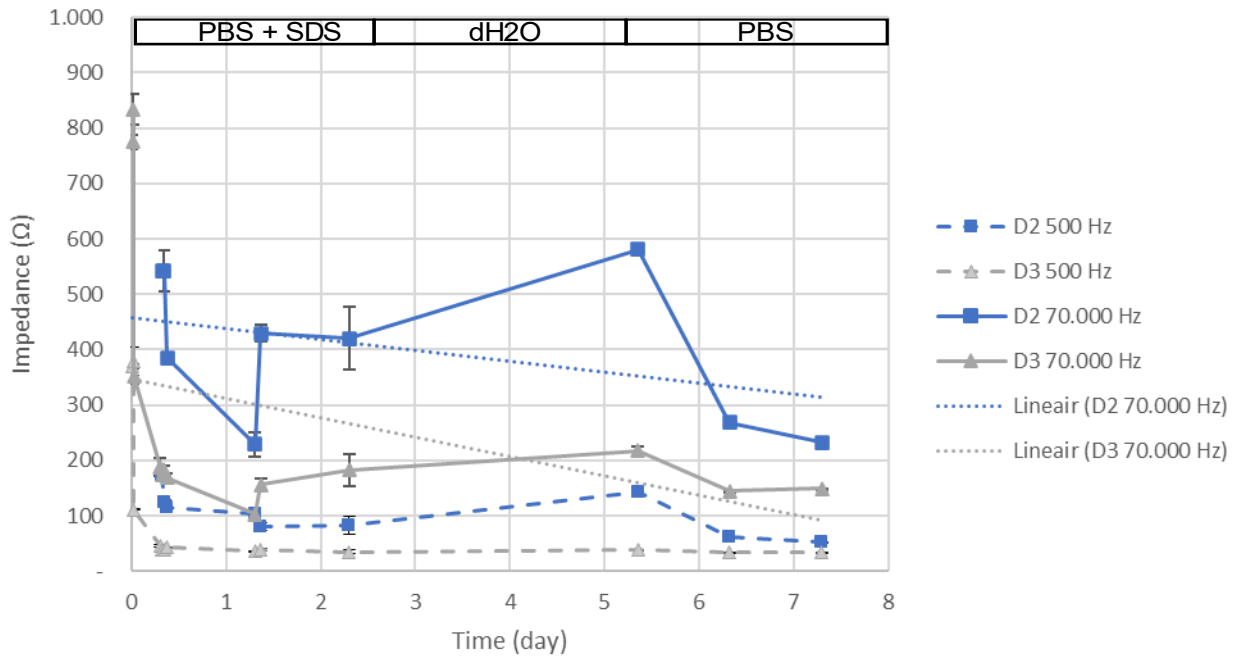
Partially decellularized measurements on kidney
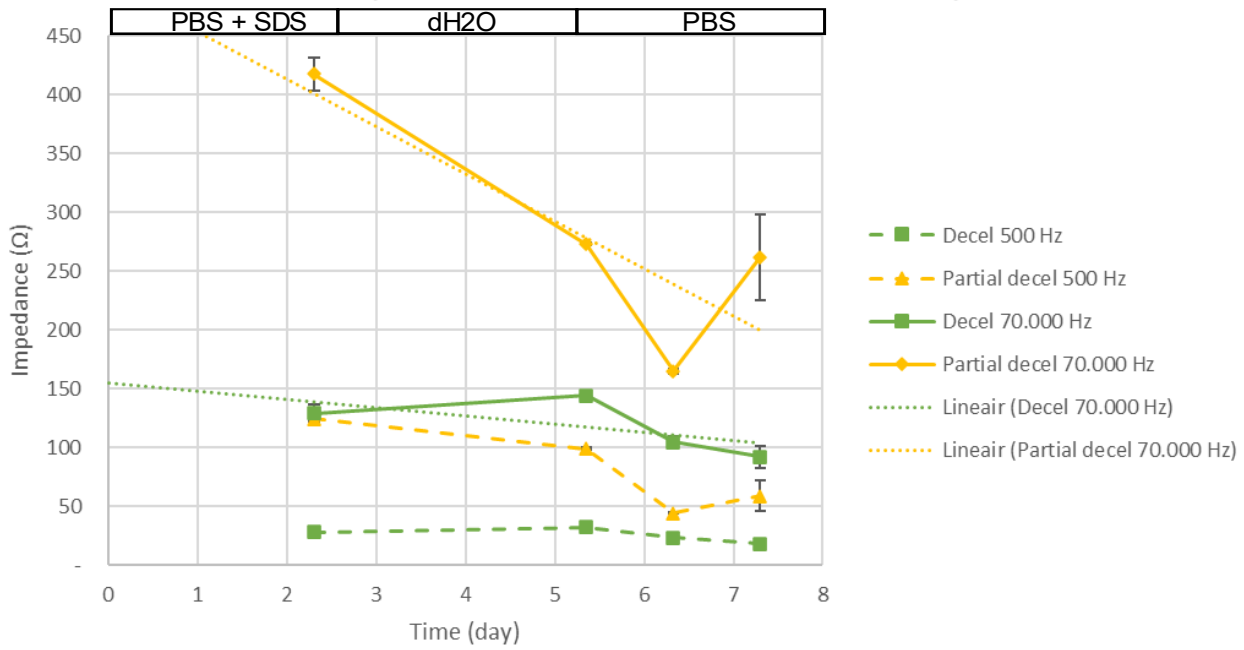
Oedema measurements through artery; Path 1 - middle

Oedema measurements through artery; Path 2 - oedema

Appendix 4 – Oedema measurements through on the kidney

Oedema measurements on kidney; Path 2 - oedema
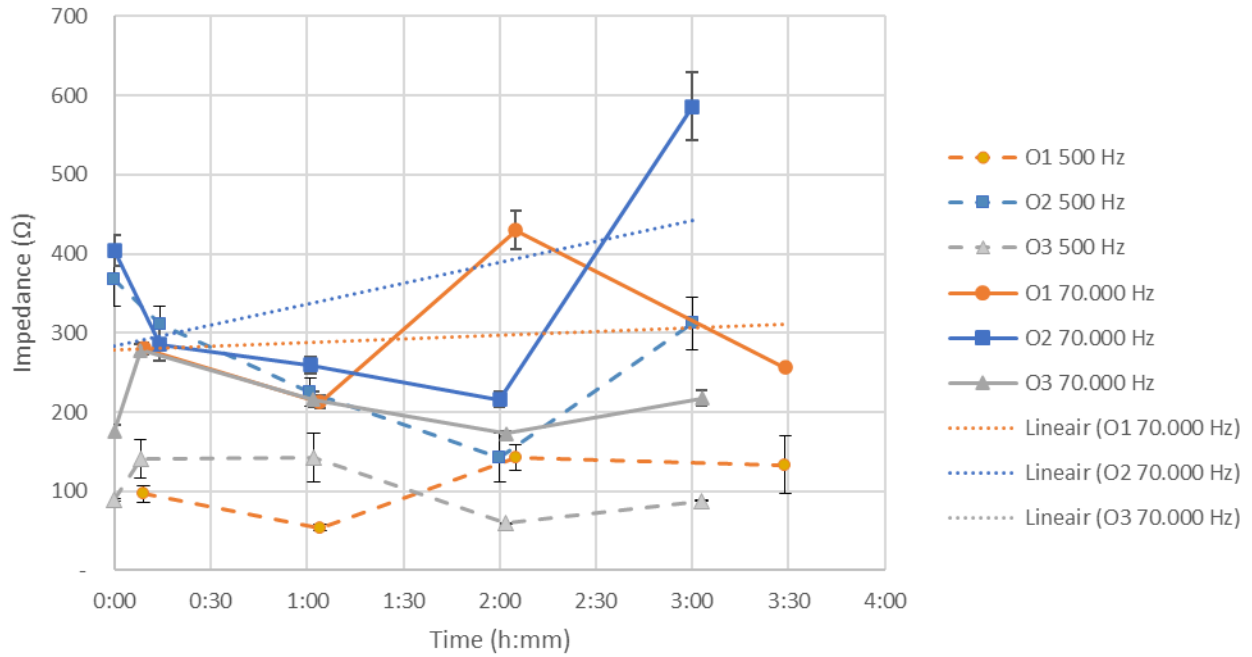
Oedema measurements on kidney; Path 3 - control
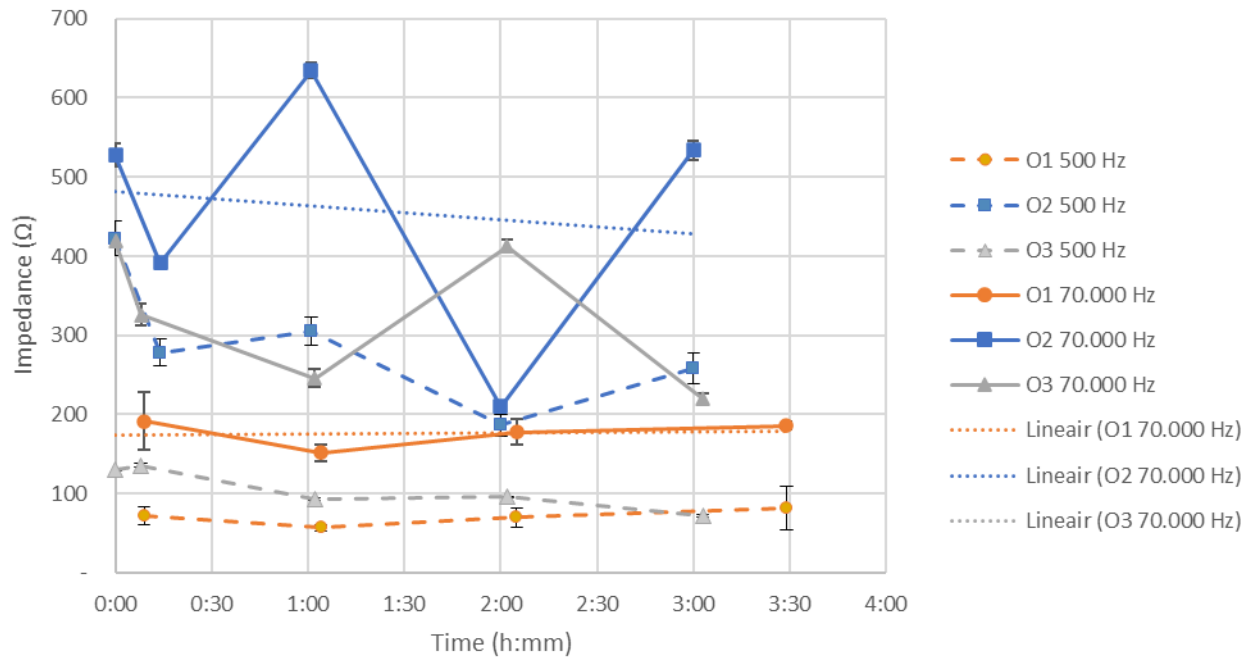
Appendix 5 – Vascular obstruction measurements through the artery

Vascular obstruction measurements through artery; Path 3 - control
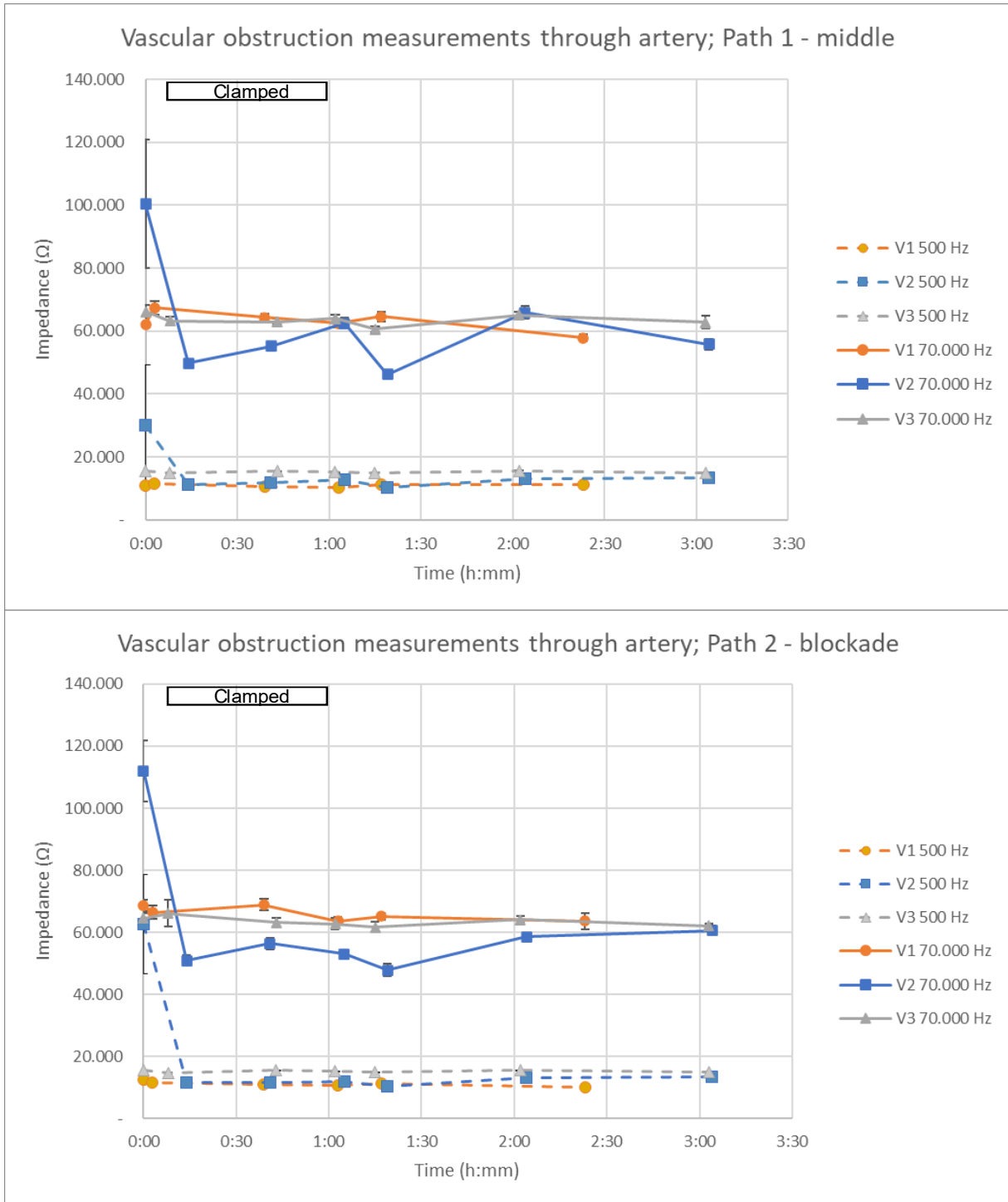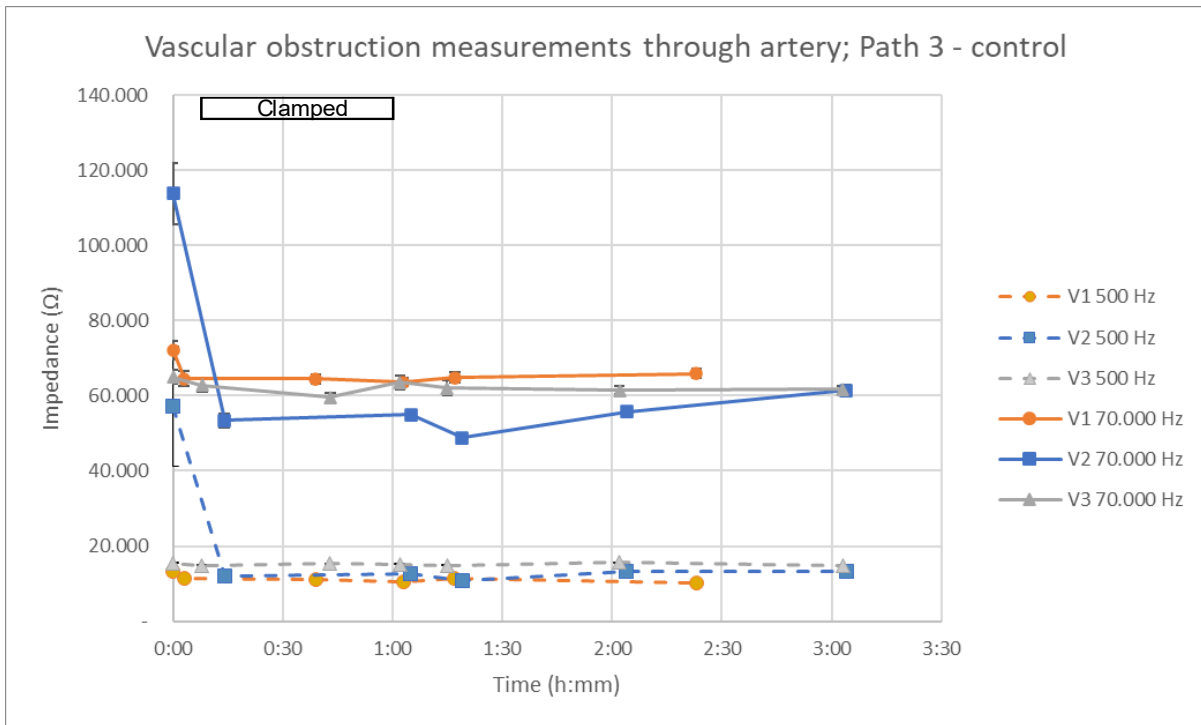
Appendix 6 – Vascular obstruction measurements on the kidney

Vascular obstruction measurements on kidney; Path 1 - whole kidney

Vascular obstruction measurements on kidney; Path 2 - blockade

Vascular obstruction measurements on kidney; Path 3 - control

Appendix 7 – Data of pressure and distance influence on impedance

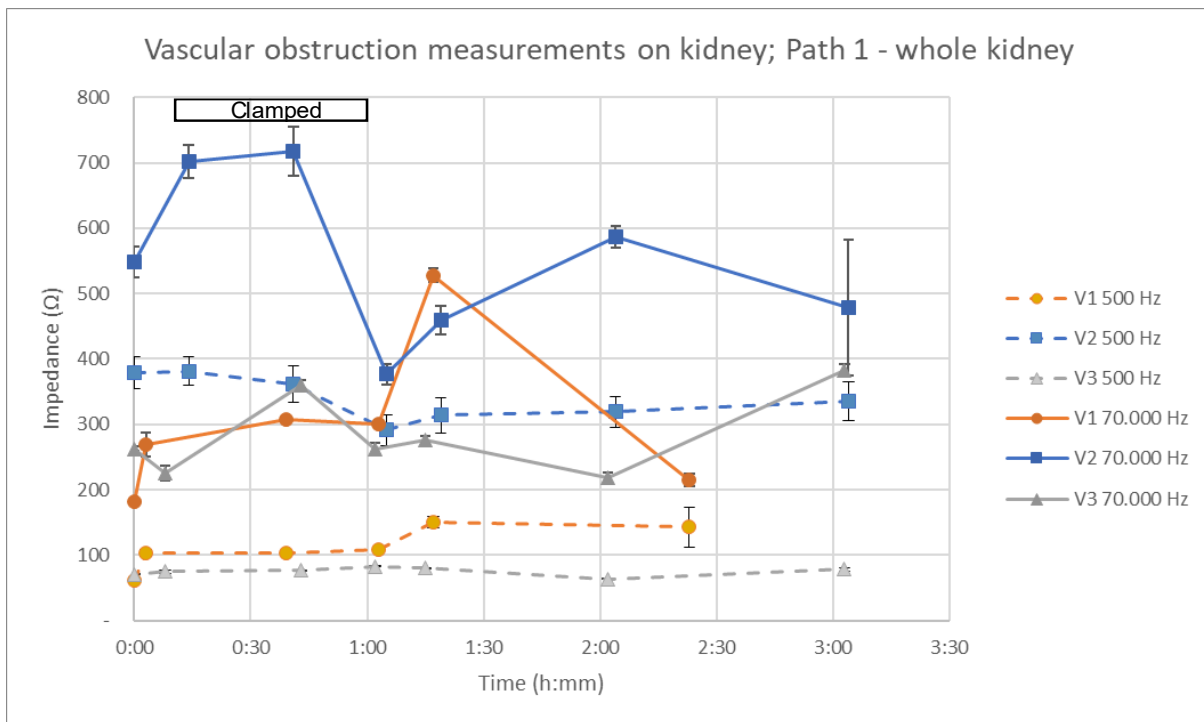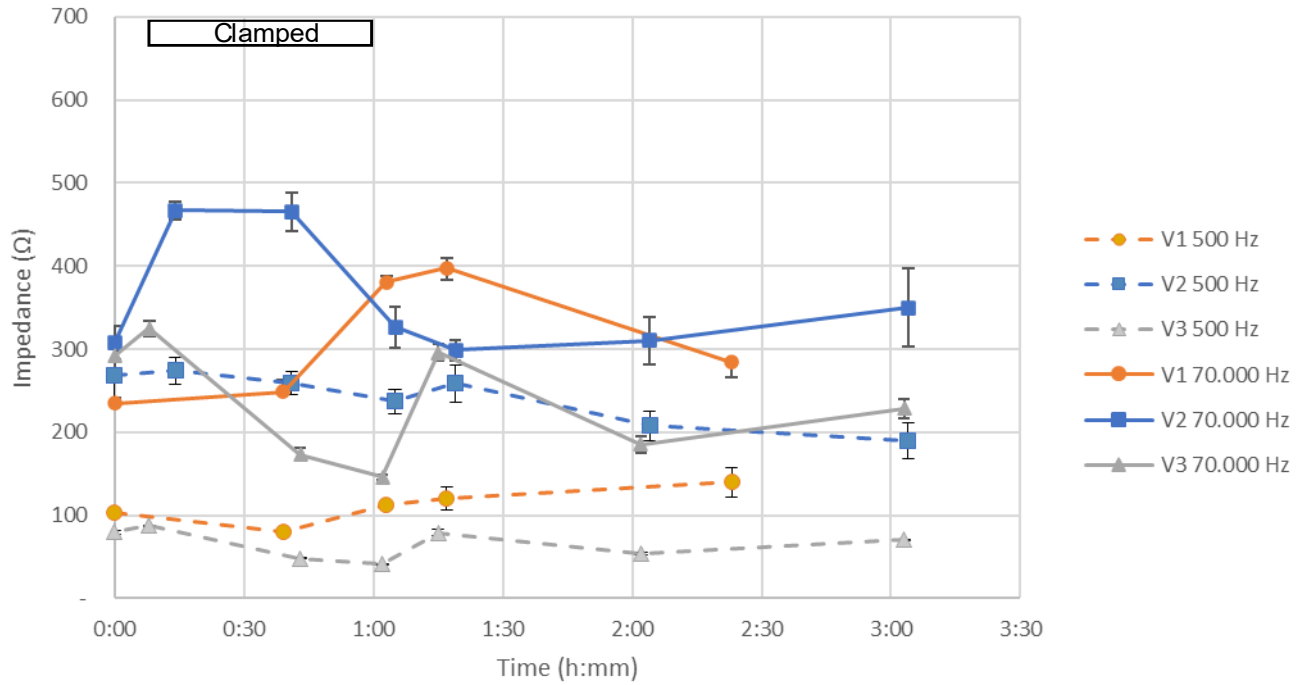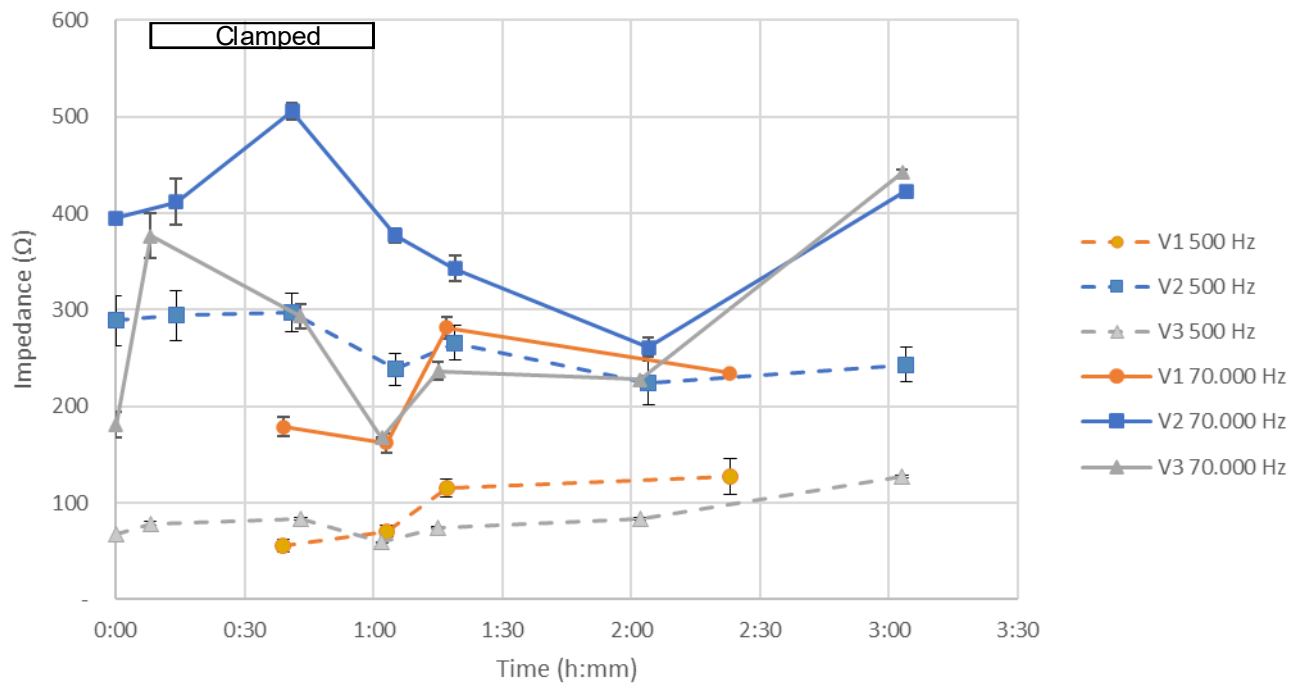| RPM, length tube	200	500	800	1.000	2.000	5.000	8.000	10.000	15.000	20.000	30.000	40.000	50.000	60.000	70.000
50 ml/min, 10 cm	8.267,24	8.189,45	8.150,97	8.135,41	8.122,07	8.161,20	8.267,64	8.381,24	8.712,47	9.388,19	11.435,48	13.366,03	16.231,83	21.010,38	29513,8542
100 ml/min, 10 cm	8.264,79	8.196,59	8.172,06	8.157,90	8.147,39	8.216,73	8.344,26	8.474,36	8.908,15	9.476,07	11.628,80	13.685,63	16.927,59	21.975,51	30980,3854
200 ml/min, 10 cm	8.253,85	8.187,14	8.148,84	8.142,76	8.130,31	8.221,70	8.356,45	8.437,97	8.901,77	9.532,86	11.608,74	13.639,71	16.824,56	21.919,06	30961,8542
300 ml/min, 10 cm	8.243,14	8.163,89	8.125,98	8.108,68	8.102,76	8.190,31	8.341,39	8.465,97	8.893,13	9.517,32	11.568,29	13.657,43	16.858,53	21.922,68	31108,3333
50 ml/min, 54 cm	19.038,45	18.918,78	18.832,71	18.819,76	18.794,22	18.969,49	19.187,71	19.453,27	20.357,54	21.333,84	23.735,52	28.795,21	33.966,19	42.976,05	58866,8958
100 ml/min, 54 cm	19.099,36	18.870,57	18.726,19	18.672,80	18.688,89	18.853,84	19.116,41	19.376,97	20.199,40	21.293,46	23.919,30	28.750,49	33.551,70	42.296,84	58799,6771
200 ml/min, 54 cm	18.833,74	18.546,73	18.380,33	17.963,36	17.927,88	18.647,02	19.000,73	19.364,97	20.333,65	21.373,67	23.882,76	29.322,66	35.862,13	44.766,91	59032,4583
300 ml/min, 54 cm	18.850,52	18.530,54	18.474,45	18.470,26	18.463,31	18.829,69	19.055,69	19.249,05	20.254,28	21.342,68	23.914,59	29.460,33	34.356,61	43.467,90	60645,3333
50 ml/min, 93 cm	29.158,51	29.053,68	28.983,31	28.939,69	28.936,47	29.013,86	29.111,91	29.338,02	30.067,95	31.102,52	33.998,38	39.878,72	44.392,67	54.394,65	73167,8438
100 ml/min, 93 cm	29.067,03	28.860,66	28.760,93	28.745,60	28.718,92	28.834,96	29.056,33	29.157,73	30.052,18	31.257,48	34.175,00	39.732,53	44.898,83	55.220,64	74151,3021
200 ml/min, 93 cm	29.462,17	29.109,49	29.030,96	28.850,63	28.750,15	29.050,74	29.792,14	29.868,61	30.594,60	31.996,05	34.933,60	40.645,49	45.415,00	55.367,57	74922,3333
300 ml/min, 93 cm	28.634,92	28.002,26	27.633,86	27.203,70	27.812,78	28.244,97	28.332,97	29.006,18	29.823,27	31.031,77	33.861,76	39.715,25	44.489,50	54.226,04	73502,2188

Influence of pressure and distance on impedance
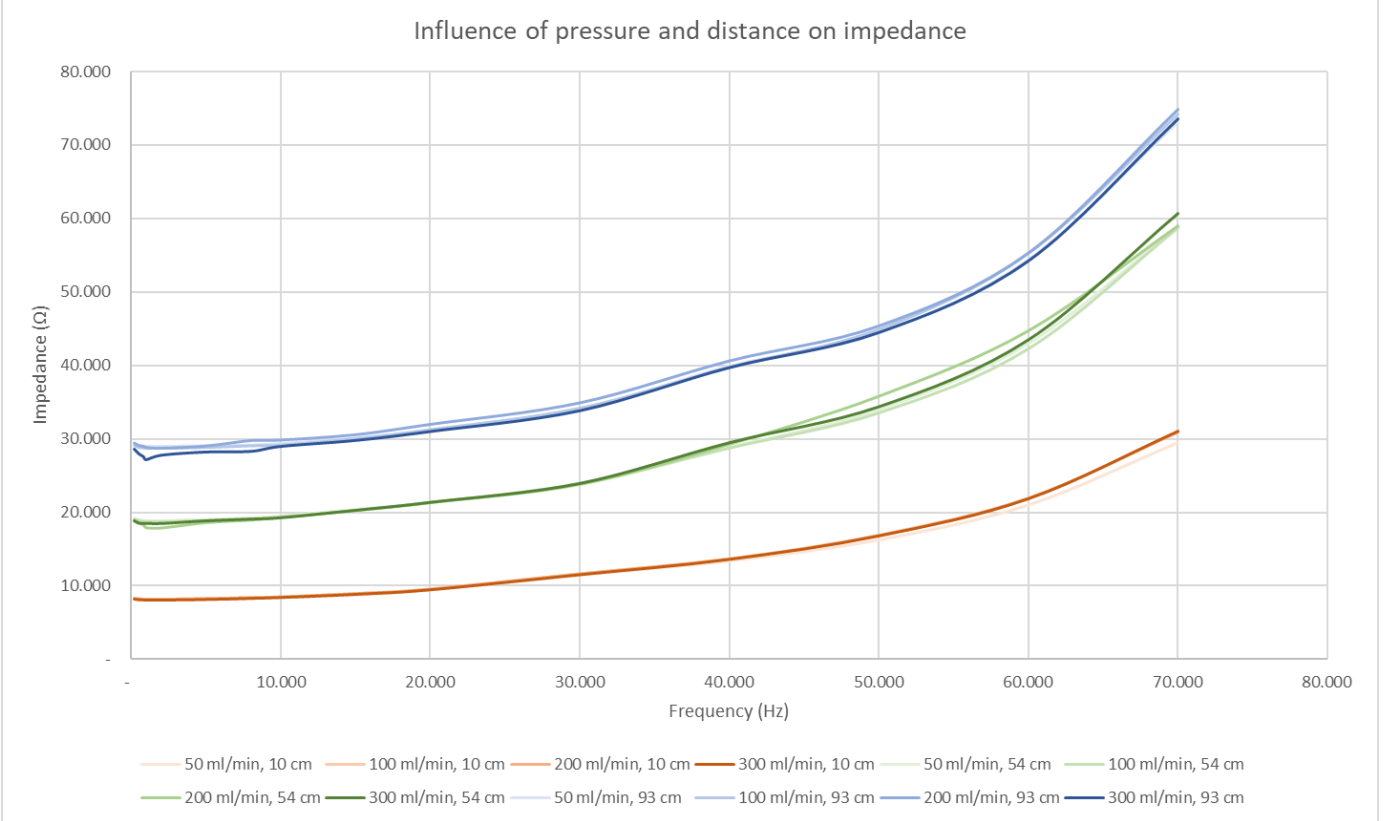
Appendix 8 – Data of impedance of the perfusate during decellularization

Kidney D2 - 500 Hz			
Time	Perfusate	Impedance	Standard deviation
00:00:36	PBS 0	11.474,8647	21,5921
00:01:05	PBS+SDS 1	9.466,8996	282,3526
00:01:22	PBS+SDS 1	9.927,8594	355,1952
00:18:03	PBS+SDS 1	9.674,2696	224,0385
00:19:32	PBS+SDS 1	#N/B	#N/B
00:20:45	PBS+SDS 1	10.795,3073	186,2569
00:22:33	PBS+SDS 2	11.006,8333	24,0059
01:18:13	PBS+SDS 2	10.583,8141	33,6412
01:22:10	PBS+SDS 3	10.533,7750	111,3964
02:18:13	PBS+SDS 3	9.885,2228	226,2842
02:20:40	dH2O 1	59.849,5639	3.347,3747
03:22:58	dH2O 1	53.762,4612	1.377,8928
05:17:30	dH2O 2	58.016,2071	3.878,3275
05:21:04	PBS 4	10.510,8397	665,6352
06:19:26	PBS 4	11.548,2617	834,4650
07:17:59	PBS 5	9.273,9858	432,7330

Kidney D3 - 500 Hz			
Time	Perfusate	Impedance	Standard deviation
00:00:36	PBS 0	8.425,2500	313,8517
00:01:05	PBS+SDS 1	9.531,7574	267,4694
00:01:22	PBS+SDS 1	10.228,3906	299,8311
00:18:03	PBS+SDS 1	9.781,6406	215,8733
00:19:32	PBS+SDS 1	#N/B	#N/B
00:20:45	PBS+SDS 1	9.534,1908	238,9378
00:22:33	PBS+SDS 2	9.910,0826	174,3517
01:18:13	PBS+SDS 2	8.970,6176	405,5245
01:22:10	PBS+SDS 3	#N/B	#N/B
02:18:13	PBS+SDS 3	9.790,5469	167,4135
02:20:40	dH2O 1	56.111,4861	2.417,8855
03:22:58	dH2O 1	51.498,1136	2.426,8746
05:17:30	dH2O 2	118.268,2095	12.049,9304
05:21:04	PBS 4	10.365,1654	1.013,5768
06:19:26	PBS 4	9.403,5347	164,7419
07:17:59	PBS 5	9.048,7695	199,1177

Kidney D2 - 70.000 Hz			
Time	Perfusate	Impedance	Standard deviation
00:00:36	PBS 0	40.618,7121	171,7641
00:01:05	PBS+SDS 1	41.790,1183	12.761,5159
00:01:22	PBS+SDS 1	39.680,7701	562,6925
00:18:03	PBS+SDS 1	37.388,7339	724,4011
00:19:32	PBS+SDS 1	#N/B	#N/B
00:20:45	PBS+SDS 1	39.672,9427	278,4475
00:22:33	PBS+SDS 2	42.069,2683	144,6332
01:18:13	PBS+SDS 2	39.221,4407	105,2626
01:22:10	PBS+SDS 3	40.112,3750	175,3792
02:18:13	PBS+SDS 3	37.943,0978	584,7399
02:20:40	dH2O 1	95.622,0340	987,0234
03:22:58	dH2O 1	92.044,1983	198,3919
05:17:30	dH2O 2	106.930,9857	1.028,6438
05:21:04	PBS 4	37.673,8152	2.608,2164
06:19:26	PBS 4	38.576,3897	1.887,9998
07:17:59	PBS 5	33.673,9233	1.157,3095

Kidney D3 - 70.000 Hz			
Time	Perfusate	Impedance	Standard deviation
00:00:36	PBS 0	37.622,7083	561,6858
00:01:05	PBS+SDS 1	35.049,6875	579,0898
00:01:22	PBS+SDS 1	37.633,2109	560,9662
00:18:03	PBS+SDS 1	36.218,0847	244,1087
00:19:32	PBS+SDS 1	#N/B	#N/B
00:20:45	PBS+SDS 1	37.173,4770	362,5496
00:22:33	PBS+SDS 2	37.387,1295	337,7689
01:18:13	PBS+SDS 2	34.202,9044	776,9203
01:22:10	PBS+SDS 3	#N/B	#N/B
02:18:13	PBS+SDS 3	35.340,0813	285,0200
02:20:40	dH2O 1	76.684,6076	575,6407
03:22:58	dH2O 1	70.872,2244	669,3880
05:17:30	dH2O 2	59.124,9688	261,0688
05:21:04	PBS 4	33.682,9429	2.575,5427
06:19:26	PBS 4	32.633,0216	4.392,3425
07:17:59	PBS 5	31.133,0993	631,5912

Impedance of the perfusate during decellularization
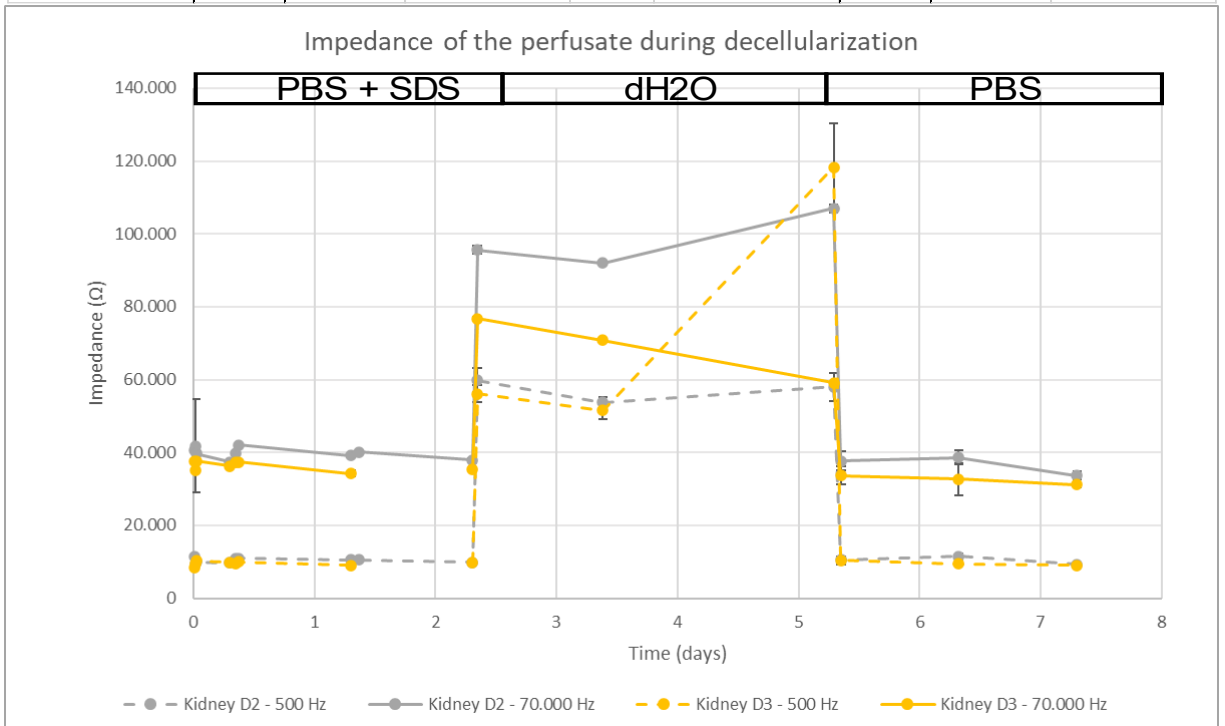
Appendix 9 – Data of impedance of three-way valves

Impedance															
Number of valves	**200**	**500**	**800**	**1000**	**2000**	**5000**	**8000**	**10000**	**15000**	**20000**	**30000**	**40000**	**50000**	**60000**	**70000**
Three-way valve 1x	9.985	9.770	9.690	9.673	9.692	9.895	10.140	10.326	10.933	11.727	13.782	17.234	21.332	27.982	39.808
Three-way valve 2x	15.464	15.115	15.141	15.171	15.180	15.431	15.789	16.126	16.978	18.241	20.593	25.838	31.382	40.250	56.730
Three-way valve 3x	22.704	22.659	22.411	22.414	22.323	22.482	22.977	23.180	24.257	25.666	29.020	35.518	41.864	52.764	72.190
Three-way valve 4x	29.932	29.917	29.842	29.811	29.893	30.098	30.337	30.701	31.729	33.338	36.925	43.643	49.791	60.956	81.724

Standard diviation															
Number of valves	**200**	**500**	**800**	**1.000**	**2.000**	**5.000**	**8.000**	**10.000**	**15.000**	**20.000**	**30.000**	**40.000**	**50.000**	**60.000**	**70.000**
Three-way valve 1x	141	154	166	178	174	161	154	154	159	164	173	229	274	338	436
Three-way valve 2x	1.512	1.419	1.355	1.456	1.420	1.486	1.486	1.507	1.510	1.497	1.840	1.899	2.013	2.149	2.553
Three-way valve 3x	1.932	1.935	1.892	1.980	1.979	1.979	1.953	1.978	1.880	2.162	2.176	2.084	1.921	2.048	2.007
Three-way valve 4x	62	18	134	169	18	74	205	129	127	125	100	137	156	229	355

Impedance per three-way valve — Impedance (Ω) vs Amount of three-way valves (#); series 500 Hz and 70.000 Hz.
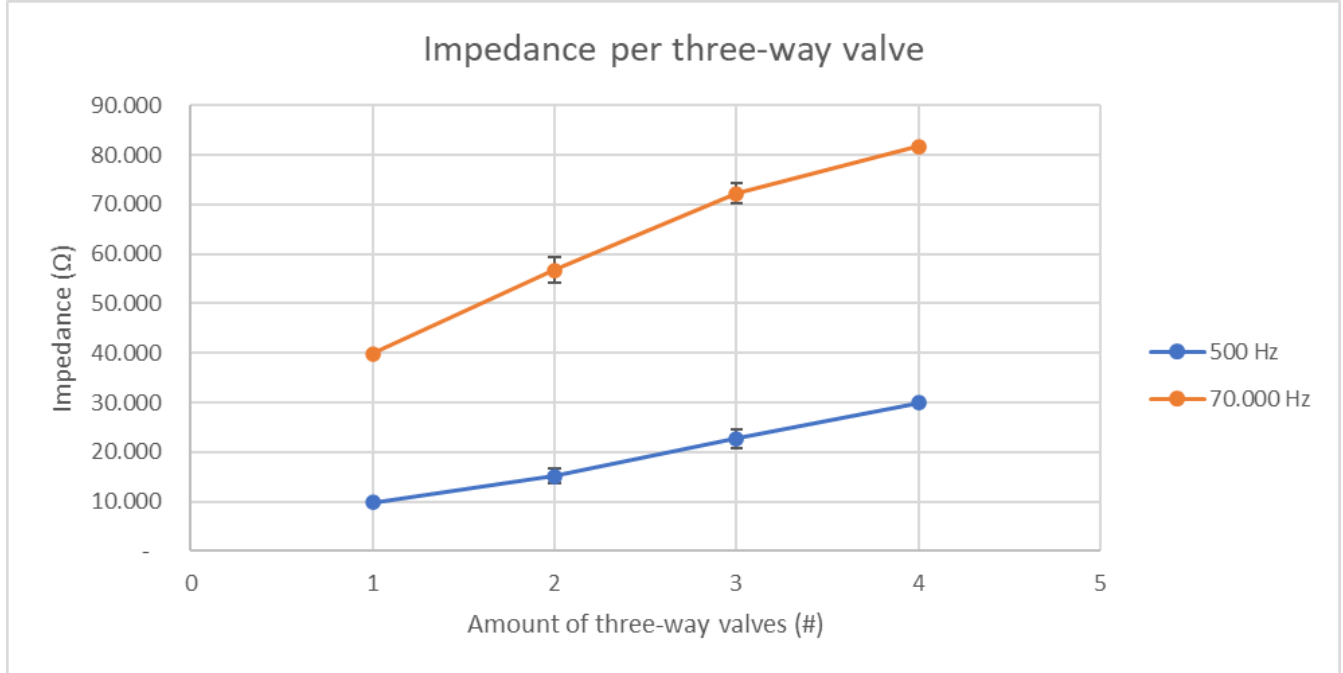
Fluid	Percentage RBC	200	500	800	1.000	2.000	5.000	8.000	10.000	15.000	20.000	30.000	40.000	50.000	60.000	70.000
PBS	0%	96,84	78,61	78,19	81,08	96,49	82,39	94,03	81,20	82,79	86,50	100,55	121,00	149,80	189,02	273,88
25/75 Blood/PBS	7,5%	129,74	114,47	114,11	117,54	138,75	118,18	134,78	117,15	118,22	122,39	140,78	167,99	206,46	267,04	361,05
50/50 Blood/PBS	15%	175,30	162,72	162,56	167,17	197,55	169,65	193,52	169,51	173,07	181,45	213,95	259,95	324,05	418,32	583,94
75/25 Blood/PBS	22,5%	186,97	173,86	171,78	176,31	207,35	178,71	202,24	178,16	181,24	189,53	220,88	264,67	328,58	423,77	583,64
Blood	30%	276,80	264,38	262,09	267,27	314,66	274,81	308,15	275,23	280,35	295,41	345,21	416,98	518,53	669,95	922,39
Filtered Blood	60%	3.843,35	3.798,18	3.794,02	3.788,10	3.801,45	3.860,19	3.963,72	4.059,74	4.356,83	4.733,81	5.652,59	6.768,22	8.089,04	9.973,35	12.996,20
Serum	0%	155,90	143,18	142,80	147,91	175,09	150,42	172,33	150,51	153,70	161,13	189,73	231,45	288,43	375,60	518,15
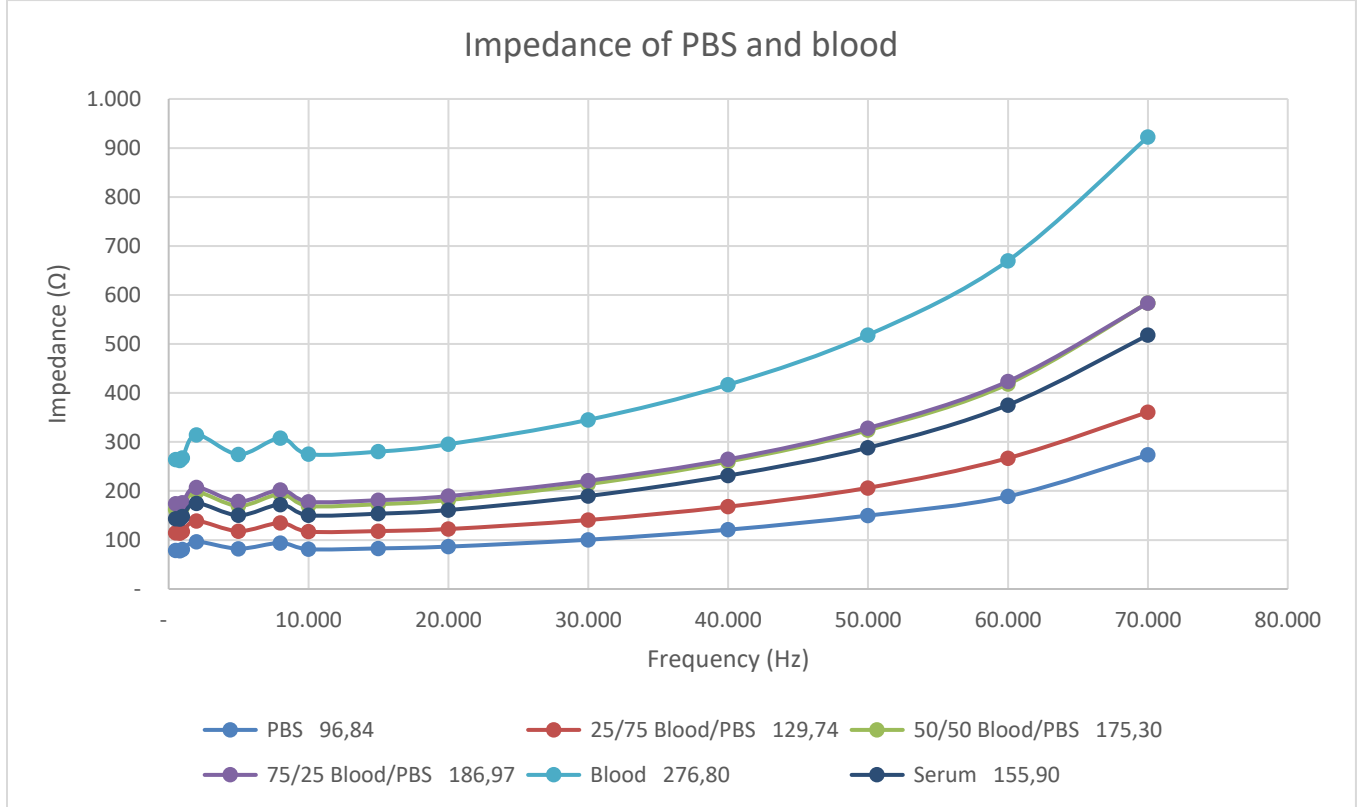
Appendix 11 – Data of impedance of porcine kidney tissue

Organ	200	500	800	1.000	2.000	5.000	8.000	10.000	15.000	20.000	30.000	40.000	50.000	60.000	70.000
Kidney 1, Cortex 3 cm	287,40	181,39	182,67	178,10	192,17	157,29	153,84	139,15	132,31	126,83	123,45	128,08	142,34	173,02	228,60
Kidney 1, Cortex 5 cm	330,60	198,96	195,79	197,19	208,38	184,01	178,86	174,05	172,43	177,60	191,42	217,99	255,74	315,72	430,10
Kidney 1, Cortex 13 cm	562,16	565,66	565,75	561,71	573,88	493,39	467,68	439,66	416,63	408,49	413,39	440,25	492,40	583,51	743,05
Kidney 1, Medula 1 cm	198,35	151,04	152,44	152,27	174,33	143,48	148,41	133,64	131,64	135,44	152,07	180,08	218,05	280,30	380,11
Kidney 1, Medula 1 cm	200,52	165,65	163,52	165,72	186,11	154,57	159,04	143,55	140,70	143,90	161,70	189,57	233,80	297,01	407,13
Kidney 1, Medula 3 cm	215,66	136,88	135,98	136,15	156,22	135,35	144,72	137,22	148,01	159,19	195,91	240,64	302,95	390,71	540,13
Kidney 1, Medula 7 cm	566,45	511,34	505,51	505,33	558,24	470,07	468,07	439,95	434,03	437,76	469,05	526,64	618,33	757,72	1.009,65
Kidney 2, Cortex 1 cm	263,90	147,13	143,32	141,57	147,10	134,97	134,93	133,18	137,71	144,58	167,11	194,59	238,89	306,44	410,77
Kidney 2, Cortex 3 cm	353,61	305,14	298,48	300,29	296,29	255,41	239,15	229,83	223,68	226,85	246,64	280,17	331,88	410,36	551,49
Kidney 2, Cortex 6 cm	443,29	384,47	375,59	380,97	371,90	369,88	367,74	368,78	381,14	400,01	456,99	540,18	654,68	821,70	1.107,79
Kidney 2, Medula 1 cm	128,95	112,88	111,49	114,21	131,14	106,24	114,70	97,69	93,69	92,64	98,67	111,45	132,70	161,76	221,35
Kidney 2, Medula 5 cm	258,78	248,80	247,47	250,58	290,11	239,50	256,70	223,65	217,09	219,78	244,36	283,13	341,94	434,89	583,40

Impedance Cortex

Impedance Cortex